DEPARTMENT OF PHYSICS, UNIVERSITY OF JYVÄSKYLÄ
RESEARCH REPORT No. 4/1997

NOBLE GASES IN COPPER

BY
JUHA KUHALAINEN

Academic Dissertation
for the Degree of
Doctor of Philosophy

Jyväskylä, Finland
November 1997

URN:ISBN:978-951-39-9758-8
ISBN 978-951-39-9758-8 (PDF)
ISSN 0075-465X

Jyväskylän yliopisto, 2023

ISBN 951-39-0093-2
ISSN 0075-465X

DEPARTMENT OF PHYSICS, UNIVERSITY OF JYVÄSKYLÄ
RESEARCH REPORT No. 4/1997

NOBLE GASES IN COPPER

BY
JUHA KUHALAINEN

Academic Dissertation
for the Degree of
Doctor of Philosophy

To be presented, by permission of the
Faculty of Mathematics and Natural Sciences
of the University of Jyväskylä,
for public examination in Auditorium FYS-1 of the
University of Jyväskylä on November 28, 1997,
at 12 o'clock noon

Jyväskylä, Finland
November 1997

Preface

This work, concerning both experimental and theoretical studies of noble gas impurities in copper, was carried out during the years 1992-1997 at the Department of Physics in the University of Jyväskylä.

I wish to express my sincere thanks to my supervisor, Prof. Matti Manninen, for encouraging discussions concerning all parts of this thesis and for valuable help when the publications were written.

I am also deeply indebted to Dr. Erkki Kautto, who has guided me during these years, especially in the field of experimental studies. All measurements presented in this thesis have been done in collaboration with Dr. Kautto.

Among many others who have helped me during these years I would like to mention Dr. Martti Puska, who guided me in the field of effective medium theory and gave the jellium program which is the basis of whole theory, and Dr. Hannu Häkkinen who helped me with the molecular dynamics.

Finally, I would like to acknowledge the financial support from the Graduate School of Material Physics, which made it possible to do this thesis.

Jyväskylä, June 1997

Juha Kuhalainen

Abstract

This thesis reviews five publications where interactions between a gas impurity and copper metal are studied both experimentally and theoretically. The experimental part includes thermal desorption measurements where a copper sample is bombarded and heated while monitoring releasing gas with a mass spectrometer. This yields usually spectra where every peak represents a different binding state of the impurity atom. New analysing methods, based on kinetic equations have been developed to extract information from these spectra. All the developed methods are tested with measured spectra in various cases. The new methods can also be applied to diffusion phenomena. Thermal desorption spectroscopy needs support from theory, since usually the origin of the peaks cannot be explained purely through peak analysis. Examples are multiply filled vacancies, vacancy clusters and heavier gas-impurities, such as argon or neon. The effective medium theory has been used to study helium, neon and argon in copper. For helium excellent agreement with the experimental results was obtained. In the cases of neon and argon equally clear theoretical interpretation of all peaks of the spectrum could not be obtained.

List of Publications

This thesis is a review of the following publications:

I E. Kautto, O-P. Kähkönen, J. Kuhalainen and M. Manninen: *Facility for thermal desorption measurements*, Nucl. Inst. And meth. B, **103** , 376-382, (1995).
https://doi.org/10.1016/0168-583X(95)00821-7

II J. Kuhalainen, M.Manninen and E. Kautto: *Helium, neon and argon in copper studied with the effective medium theory*, J. Phys. Cond. Matt., 8, **49**, pp. 10317-10326 (1996)
https://doi.org/10.1088/0953-8984/8/49/022

III E. Kautto, J. Kuhalainen and M. Manninen: *Analysing methods for thermal desorption spectra*, Physica scripta, 55,**5**, pp. 628-634 , (1997)
https://doi.org/10.1088/0031-8949/55/5/016

IV E. Kautto, J. Kuhalainen and M. Manninen: *Helium neon and argon desorption from copper* , J. Phys. Cond. Matt., 9, **21** pp. 4365-4376 (1997)
https://doi.org/10.1088/0953-8984/9/21/004

V J. Kuhalainen, M. Manninen and E. Kautto: *Argon and neon trapping near copper surfaces*, submitted to J. Phys. Cond. Matt.
https://doi.org/10.1088/0953-8984/10/21/007

The author of this thesis has written the papers II, IV and V. Paper III is written in co-operation with Dr. E. Kautto. The author has developed the peak area method and the numerical integration method, tested all introduced methods with measured data and done all experimental measurements in co-operation with Dr. E. Kautto. The author has also written the main part of the used computer programs and calculated parameters for neon and argon in copper, and made all the total energy calculations that are described in papers II and V.

Table of contents

1. Introduction

Properties of solid materials can be controlled by means of ion beams. This has both fundamental and technological interest. Examples of that are ion coating of metals for better wear resistance, sputtering of the surfaces for removing impurities, and creation of impurities and defects in semiconductors. One branch of this is nuclear materials engineering. In this research area properties of the materials under irradiation are studied and research concentrates on pointlike defects, which are for example impurity interstitials, vacancies or small clusters of these. Main part of the research is done for gas impurities since these particles are generated in some fission and fusion reactions [1]. It is also observed that gas impurities form bubbles that can lead to surface blistering [2]. Therefore a good understanding of fundamental properties of those defects is of great importance in many areas of physics.

Defect properties and impurity-defect interactions are investigated by a number of experimental and theoretical methods: resistivity measurements, channeling, nuclear reaction analysis, positron annihilation, Rutherford backscattering, perturbed angular correlation, thermal desorption and a wide variety of computer simulation methods. These methods can give suggestions about the processes that are present in lattice when it is irradiated. Usually the most interesting quantities to be determined are the number of vacancies and other defects created in irradiation and activation energies for dissociation and migration. One of the modern methods is thermal desorption spectroscopy which can give direct information about these quantities. It was introduced by Kornelsen and co-workers at Delft [3-4], although general desorption phenomena has been known for years before and similar works has been done elsewhere [5]. In this thesis thermal desorption as well as computer simulations are used to study the behavior of light noble gases in copper.

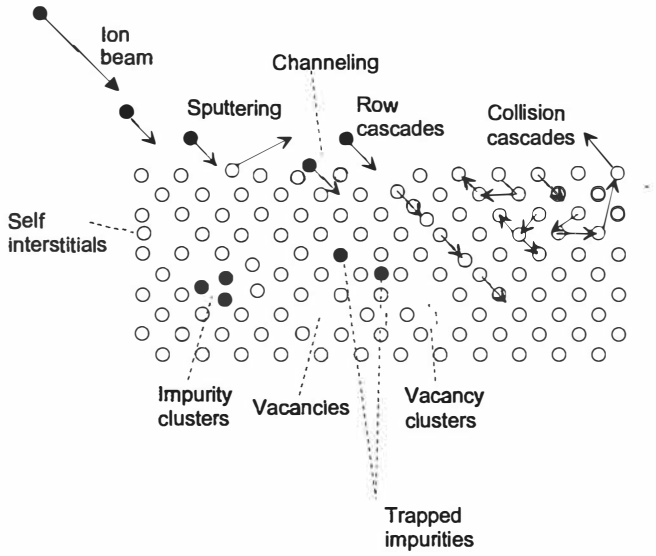

Figure 1.1. *Irradiation of a solid target with ion beam. Collision cascades create vacancies and leave impurity atoms in crystal. When irradiation doses and energies are sufficiently high, clusters of impurity atoms and vacancies are formed.*

Desorption means usually phenomena where atoms are escaping from a solid surface. The process is always activated, which means that energy must be supplied to atoms at the surface before they can escape. Energy can be supplied with a laser pulse, electron gun, heating etc. The activation energy for surface desorption of impurities is usually of the order of one meV. An other case is the desorption of noble gas atoms trapped at vacancies in the bulk. In this case the activation energies are usually measured in eV:s. The desorption from the bulk can give information of radiation effects and impurity host atom interactions in solid lattices. Simplest impurity atoms for desorption studies are noble gases because they do not form bonds with the host lattice. Helium is perhaps the best one because its diffusion energy is relatively small and it is insoluble in metal lattices.

The physical picture of an atom trapped in a lattice vacancy is quite clear. The atom moves back and forth in a potential well. When the atom gets more and more energy, it vibrates with increasing frequency until it has enough energy for

escaping from the vacancy.

However, the energy needed to release a helium atom from vacancy is of the order of one eV while the thermal energy at temperatures where helium seems to desorb from vacancies is only 50 meV. So we must use statistical description which leads to rate equations similar to those used in chemical processes. The rate equations are dependent on concentrations, vibrational frequencies, energies and temperatures and they can explain the low temperatures needed to release impurities from defects.

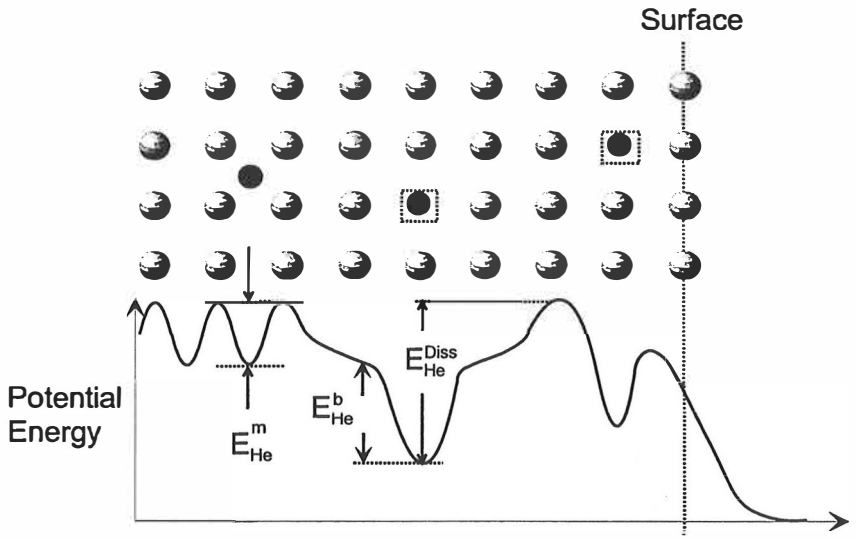

Figure 1.2. *Schematic representation of the potential energy of an impurity atom in different lattice sites. The potential well is lower when impurity is trapped near the surface.*

Rate equations are commonly used in chemistry. A rate equation describes how the concentrations of the species involved in the chemical reaction are changing. If a generic chemical reaction is expressed as $A+B+\ldots \rightarrow G$, and the concentrations of species are denoted by [A], [B], and so on, the rate of the formation of the end

product can be expressed as

$$\frac{d[G]}{dt} = \alpha[A][B]\ldots \tag{1.1}$$

where α is the rate constant. This form is purely empirical. The kinetic order of the reaction is defined to be the sum of powers of participant concentrations. In the example above, the kinetic order is the number of the species needed in the reaction, since all the powers are 1. With this example, it can be understood that the reaction is a first order reaction if formation rate of the product depends only on one concentration. The reaction order is two if two species are needed to form one end product, and so on. The reaction rate depends also on other variables, for example, on the temperature and on the activation energy. It can be shown that dependence of the rate constant on these variables is of the Arrhenius type:

$$\alpha \propto \nu e^{-E_a/k_B T} \tag{1.2}$$

where k_B is the Boltzmann constant, E_a the activation energy of the reaction and ν a frequency factor. This dependence can be derived, for example, by means of the kinetic gas theory and the collision probabilities of atoms. When the above concepts are used to describe desorption phenomena, the number of atoms in the system, N, is used instead of concentrations. With this in mind, the rate equation for desorption can be written as

$$-\frac{dN}{dt} = N(t)^m \nu e^{-E_D/k_B T} \tag{1.3}$$

In a desorption process the order of the reaction, m, is one if independent atoms are released from the surface or from the defects. The reaction order is two if two atoms are needed for the process. For example, the desorption of a helium atom from a vacancy filled with two helium atoms is expected to be of the second order since the process need two atoms.

In a typical desorption experiment the sample is heated linearly with time, $T = T_0 + \mu t$, and the amount of the releasing gas is measured as a function of the temperature. Due to this, it is useful to change variables, which gives a suitable form of the rate equation to be used in the description of the desorption

$$-\frac{dN}{dT} = \frac{\nu}{\mu}[N(T)]^m e^{-E_D/kT} \tag{1.4}$$

The escape of an atom trapped at a potential well occurs because the atom receives kicks from substrate atoms due to the thermal motion. Consequently the frequency factor can be related to the vibration frequency.

Measurements of noble gas desorption consist of three or four separate steps [6-8]

1. First a single crystal sample is sputtered with argon and annealed in ultra high vacuum for cleaning the surface from impurities and defects.
2. The next step is the bombardment of the sample with noble gas ions. Energies are usually 1-10 keV. This creates vacancy type defects to sample and leaves a gas concentration in the sample.
3. After that helium can be injected to the sample with small energies (200-300 eV). A helium beam with so a small energy cannot produce any defects to the sample but existing vacancies will be filled with helium atoms. This step is optional.
4. The last step is sample heating. Gas atoms trapped at different defects will be released at different temperatures.

The resulting desorption spectrum can have several peaks. Every peak in the spectrum indicates a different binding state of the gas atom in the lattice. The highest peak in the spectrum comes usually from singly occupied vacancies. The explanation of the smaller peaks can be clusters or vacancies that are filled with two or more helium atoms. If there are impurities at the surface of the sample they can cause additional peaks and the spectrum might become unclear. This means that all steps of the measurement have to be done in ultra high vacuum conditions and requirements for measuring equipments are high [6]. Also the sample handling and cleaning are extremely important.

An analysis of the desorption spectrum with suitable peak analysing methods gives frequency factors and activation energies for the desorption [9]. These quantities give information about the impurity-host atom interactions. Even more information is obtained if the angle of incidence, dose, heating rate and implantation

energies are varied in a systematical way in different experiments. If the mass spectrometer is well calibrated it is also possible to estimate the number of vacancies in the lattice [6]. Desorption measurements can also give information of chemical reactions that can occur if there are impurity atoms in the lattice. This is important if we want to study radiation damage in lattices or if the information is needed for sputtering or ion implantation purposes. Another important reason for desorption measurements is that theoretical potential models created for metal-impurity interactions can be tested and more accurate models can be created.

In this thesis desorption phenomena have been studied also with theoretical model calculations [10]. The theory is needed especially in the cases where desorption spectra show peaks which are overlapping or unclear, because then an interpretation of all the peaks is usually not possible by means of measurements alone. For doing the calculations, reliable interatomic potentials are needed. At the moment it is not possible to apply accurate *ab initio* methods when modelling noble gas behavior in metal, since the number of atoms needed in one calculation is typically few thousand. There are however some accurate many-body potentials available, like the effective medium theory (EMT), which can be used in these model calculations [11-14]. The main aim of the present calculations is to determine energetics of different processes that are present when thermal desorption experiments are done. Especially, we want to know dissociation, formation and migration energies of noble gas impurities in copper. In this work we have utilized a special form of the effective medium theory, which allows to have several different atomic species interacting with each other [11].

The plan of the thesis is as follows. In section 2 the experimental setup is shortly described. Section 3 describes the experiments and gives the experimental results. The analysing methods of the desorption spectra are studied in section 4. Section 5 describes the theoretical work based on the effective medium theory. The identification of the measured peaks with help of the theoretical work is discussed in section 6. The conclusions are given in section 7.

2. Experimental setup

2.1 Overall structure of the desorption spectrometer

This chapter describes shortly the thermal desorption spectrometer that was build in the accelerator laboratory of University of Jyväskylä during the years 1989-1993. This facility is described detailed in paper I and in the PhD thesis of Erkki Kautto, who took the main responsibility in constructing the facility. During this work a cold finger and a calibration system was added in the facility.

The main parts of the desorption spectrometer, shown in the figure 2.1, are the operation and desorption chambers, vacuum pumps, mass spectrometer, pressure sensors, computer, ion guns, sample manipulator and gas inlet valves [20].

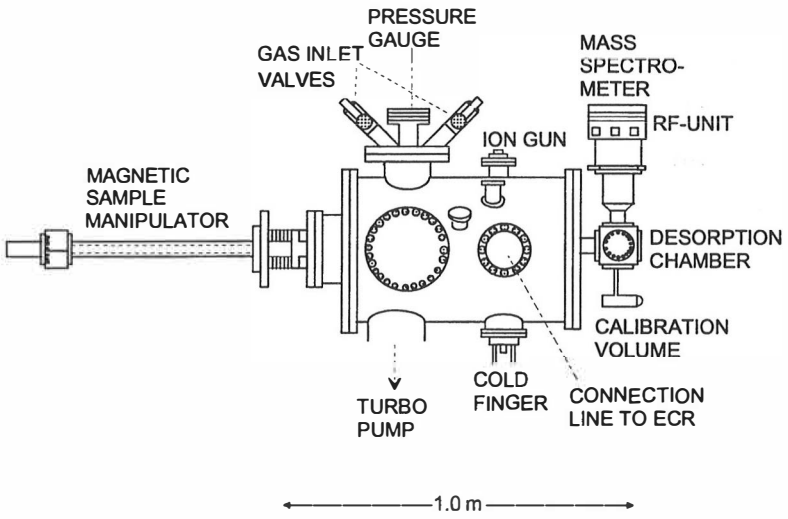

Figure 2.1. *Main parts of the thermal desorption spectrometer.*

When heat is applied to the sample, impurities are released from the surface and from traps located deeper in the crystal. This causes increase in partial pressure of the element in question. Pressure increase can be measured with a mass spectrometer. The release rate of the impurities is connected to the measured partial pressure with the equation[6,18]

$$\frac{dN}{dt} = \frac{V}{k_B T}\left[\frac{dP}{dt} + \frac{P}{\tau}\right] \tag{2.1}$$

where V is the volume of the desorption chamber, t the time, T the temperature, P the measured partial pressure and $\tau = V/S$ is the pumping time constant while S is pumping speed of the desorption chamber. If the pumping speed is small the second term in the right hand side of equation 2.1 is small and the spectrometer operates in the static mode. In this case the release rate is proportional to the pressure change in the desorption chamber. If the pumping speed is high the term (P/τ) dominates and the release rate is proportional to the pressure. Usually the dynamic operation mode is preferred because peaks can be resolved more accurately when they can be determined directly from the pressure.

2.2 Vacuum conditions and calibration

The desorption of the impurities implanted in the sample are detected with a mass spectrometer. Therefore main requirements for the desorption spectrometer are pure samples and ultra high vacuum (UHV) conditions [21-23]. This means that the total pressure in the operation chamber can not be higher than about 10^{-8} Pa. Since quantities of the releasing impurities are small (usually $10^{10} - 10^{14}$ $atoms/cm^2$), the background pressure for those species has to be small. In the case of noble gas measurements this can be achieved with one turbomolecular pump because noble gases are minor parts in the residual gas. If the measured impurity is hydrogen or oxygen then two or more pumps are needed and the volume of operation chamber has to be small.

In our spectrometer the operation chamber volume is 35ℓ and it is pumped with one turbomolecular pump. The pumping speed is $450\ell/s$. For the actual desorption

measurements the sample is moved to a measurement chamber which a volume of only 300 cm^2. Residual gas analysis show that the main component normally present in the operation chamber is hydrogen. This is clear since the turbomolecular pump is not so effective for lightest elements and hydrogen is also large component in air. Other impurities in the residual gas are carbon oxide, water and oxygen. These impurities are however minor parts in residual gas.

In order to get quantitative estimates of the number of released atoms the spectrometer has to be calibrated. We constructed a simple calibration system consisting of a single angle valve. Closing one end of the valve leaves a small known volume which can be used for the calibration. First the gas pressure of the entire desorption system is increased to a wanted value by a leak valve. Then the leak valve and the angle valve are closed, the operation chamber and desorption chamber are pumped empty, and finally the angle valve is opened and the response of the mass spectrometer is recorded. Because the volume of the calibration chamber and the gas pressure are known, the calibration can be done easily by calculating the number of the atoms that were in the calibration volume. The calibration shows that the integrated area of the measured peak is accurately proportional to the number of released gas atoms.

The same procedure is used also when the pumping time constant is determined (equation 2.1). This can be done by assuming that the partial pressure of the measured impurity is a sum of the background pressure and the pressure that is caused by the gas released from the calibration volume. The time needed to decrease the pressure to the background level gives this time constant. More accurately this can be done by fitting the decreasing side of the measured pulse to the equation $I = I_0 \exp(-t/\tau) + I_b$ where I_b is background level of the pulse and τ is the time constant [20]. In our spectrometer the measured pumping time constant is $\tau = 0.1\ s$, which indicates that the spectrometer operates in the dynamic mode.

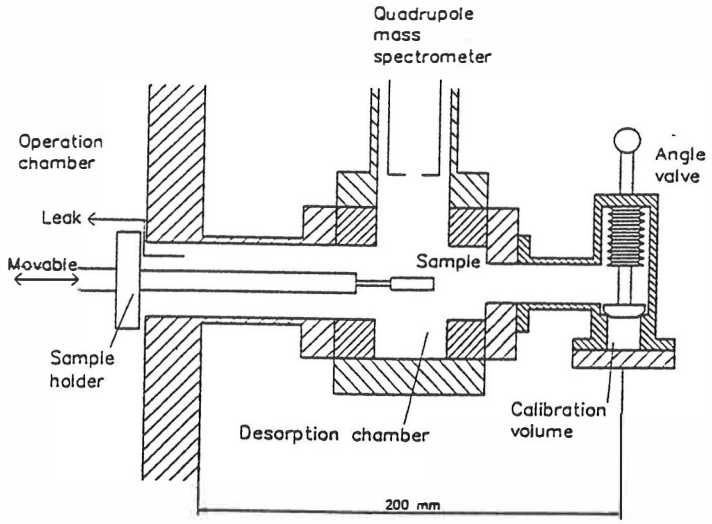

Figure 2.2. *Schematic presentation of desorption chamber, calibration volume and sample support which is movable* [20].

2.3 Irradiation facilities

Ion sources are needed for gas implantation, irradiation and sample sputtering purposes. We have used two different ion sources. Most of the measurements were done with a gas ion source connected directly to the thermal helium desorption spectrometer facility [6,20]. The gas ion source operates with the electron-impact principle, which involves a hot filament and an electric field to accelerate ions. Due to this fact the ion source can produce only gas-ion beams. The energy of the ion beam can be varied from 100 eV to 3.0 keV, which is a good energy range for sample sputtering and ion implantation. When the needed ion doses are of the order of 10^{13} $ions/cm^2$, a typical irradiation time is of the order of few minutes. Due to the lack of mass analysis the beam of the gas ion source can have impurities as well as multiply-charged ions. However, during this work no effects that could have been associated to these faults of the ion source were observed.

The other ion gun used is an electron cyclotron resonance (ECR) ion source which is the main ion source of the local cyclotron. Construction of this ion source is such that the ion beam can be turned to the THDS-facility when needed. The ECR ion source can produce a large variety of ion beams with up to few hundred keV, depending on the charge state. With this ion source it is also possible to produce different isotopes from selected elements. For example, in this work we have also used ^3He beams [24]. Most of the Ar and Ne experiments, part of the ^4He and all ^3He experiments were done with the ECR ion source.

2.4 Heating and cooling units

The preferred method for sample heating is usually electron irradiation onto its rear face. In our spectrometer the heating is, however, arranged with a resistive filament that is located under the sample in a boron-nitride oven. This gives satisfactory heating and it guarantees homogeneous temperature distribution in the sample. Estimated power need for the temperature range 200K - 1000K is 50 W at maximum [6,20]. The heating rate can be as high as 50 K/s, although lower rates are preferred for accurate measurements. The temperature of the sample is measured with K-type Chromel-Alumel thermocouple. This is the only way to do it, since the sample has to be cooled to low temperatures when irradiated. Accuracy of the temperature measured with the thermocouple is of the order of 2 K. This is enough for desorption measurements. Heating processes are controlled with PID-unit (Eurotherm 818 P), which is connected to the thermocouple, heating filament and to the power supply. The system provides smooth, programmable heating cycles that are needed in the experiments.

In some experiments also sample cooling is needed. This is arranged with a movable cold finger that is filled with liquid nitrogen. When cooling is needed during the irradiation, the cold finger is moved to contact with the boron nitride oven that supports the sample. The lowest temperature achieved with the cold finger is around 150 K. This is below the stage III in copper , where monovacancies become mobile [25].

2.5 Sample preparation and surface orientation

Single crystalline copper samples used in thermal desorption experiments were delivered by the metal laboratory of Outokumpu Copper Inc. These samples were polished both mechanically and electrolytically and the purity is 99.999%. The sample orientation was not known when the samples were shipped. The size of the samples used are $10\ mm \times 10\ mm \times 1\ mm$.

Before the samples were mounted to the sample holder in vacuum, a few images of the surface were taken with an atomic force microscope (AFM) and the surface orientation was determined. The AFM images showed that surface was smooth after the polishing. The resolution was not good enough to resolve the surface orientation

The surface orientation of the crystal was determined by using x-ray diffraction. The experiment was done with constant incoming angle. Figure 2.3 show the basic principle of the surface orientation determination with Bragg's reflection. Angle of the incoming beam (α) was 7° while scattered beam angle (β) was 110° with respect to surface. The diffraction peak was obtained at an angle 117° in the spectrum. Bragg's condition gives $d' = 0.9034\mathring{A}$ for the scattering surface. This corresponds to the (400)-surface. Now the normal of the sample surface forms an angle of $\phi = 51.5°$ with the normal of the scattering surface, since incoming and outcoming angles must be equal in the scattering plane. The angle between two different surfaces is given by

$$\cos\phi = \left[\frac{(xh + yk + zl)}{\sqrt{x^2 + y^2 + z^2} \cdot \sqrt{h^2 + k^2 + l^2}}\right]$$

This implies that the surface orientation of the sample is (340). The same measurement was done with different incoming angles and the same result for the surface orientation of the sample was observed.

Before starting measurements the sample was sputtered with argon and heated several times to 1000 K for removing argon impurities and possible oxidation from the surface.

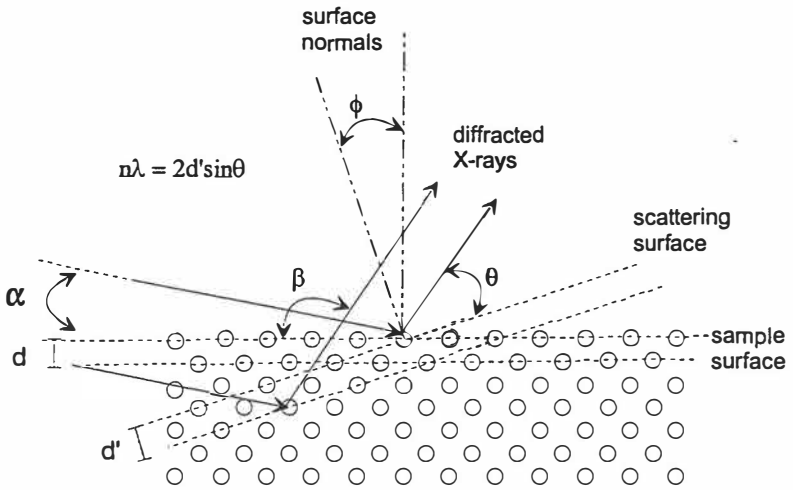

Figure 2.3. *Determination of surface orientation with X-ray diffraction.*

2.6 Penetration ranges of ions

Our desorption facility has no device for implantation depth profiling and it can not be extracted from the measured desorption data either. The implantation depth is not important when normal desorption measurements are done. In some cases it is however useful to know what are the mean penetration ranges of implanted ions or where is the maximum of the vacancy distribution created in irradiation. One such situation is so-called probing measurements where helium is implanted to existing vacancies. In such measurements desorption yields or measured intensities are much higher if the implantation profile maximum and the vacancy distribution maximum are at same depth and the corresponding profiles are overlapping. Estimates of penetration ranges are also useful when different desorption peaks are predicted or analyzed.

In this work we did the implantation energy optimization and penetration depth estimations with the computer program TRIM [26]. Although this program is

not meant for single crystalline targets, it gives at least some estimates about the quantities of interest. The program is used worldwide and it is generally accepted that results are satisfactory also in the case of crystalline targets.

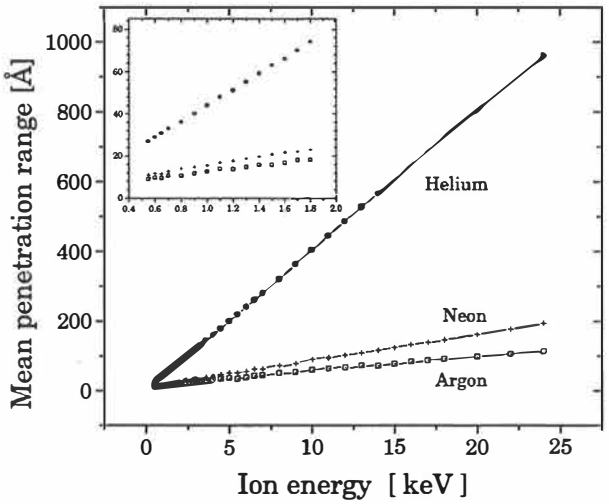

Figure 2.4. *Mean penetration ranges of helium, neon and argon in copper as a function of irradiation energy, as estimated with TRIM.*

Penetration ranges that were estimated with TRIM are shown in figure 2.4 with irradiation energies in the range of $0.5 - 25.0$ keV. As expected, helium ranges are largest since it is lightest of those noble gases. Argon penetration range is much lower due to the size and mass of the atom. For example mean ranges with 1 keV irradiation energies are 13 $\AA$ for argon, 16 $\AA$ for neon and 44 $\AA$ for helium when the angle of incidence is $0°$. The ranges for argon are low, since it transfers energy effectively to the target. Consequently argon beam produces more vacancies and other defects to the lattice than lighter atoms.

TRIM was also used to estimate vacancy profiles that were created for probing experiments. This is useful, since if these profiles are known, implantation energy of the probe atom can be optimized. Figure 2.5 shows estimates for vacancy profiles

and for impurity distributions when copper is irradiated with 1 *keV* helium, neon or argon beams, with incoming angle 30°. For the heavier ions, the maximum of the vacancy distribution is nearly at the surface. Maximum of the vacancy distribution is seen at depth 10 *Å* in case of argon and neon and around 25 *Å* in case of helium. If helium atoms are used to probe vacancies created with heavier noble gas beams, the implantation energy should be very small.

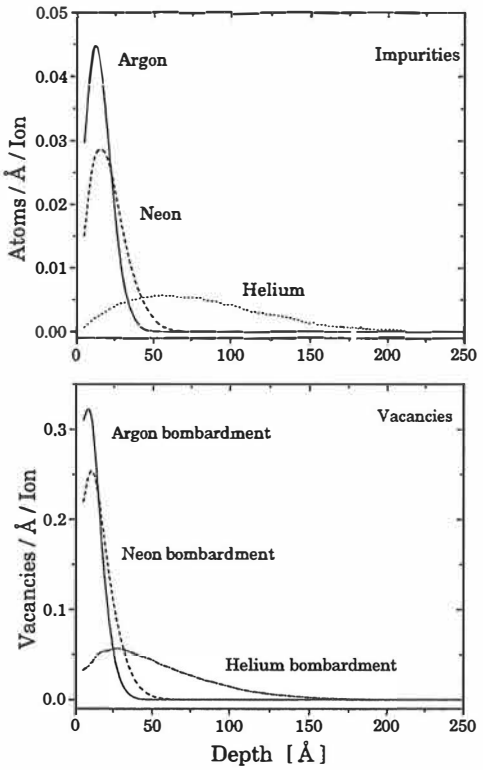

Figure 2.5. *Impurity and vacancy distributions that are created when copper is irradiated with helium, neon and argon beams. Irradiation energy is* 1 *keV and beam incoming angle is* 30° *with respect to surface normal. Profiles are calculated with TRIM.*

3. Thermal desorption measurements

In this thesis the desorption facility was used to study noble gases in copper. As explained earlier, a single crystalline copper sample was bombarded with helium, neon and argon beams, the sample was heated resistively and finally the releasing gas was measured with a mass spectrometer as a function of the temperature. These measurements give large amount of data and information about the impurity-lattice interactions and radiation defects created in bombardment. Different quantities such as the irradiation dose, the implantation energy, the implantation angle and the beam type were varied systematically. In the case of helium a clear picture of different interactions and possible phenomena was obtained. Heavier gas interactions turned out to be more difficult, but at least some peaks could be identified and explained [24].

3.1 Helium desorption from copper

In helium desorption experiments the copper sample was irradiated with a helium beam using different doses, energies and incoming angles. Irradiation doses were in the range of $10^{12} - 10^{14}$ $ions/cm^2$ while energies were varied in the range of 0.1 keV – 10.0 keV. These bombardments were done with two different ion guns described in the previous section. Low energy beams ($0.1 - 3.0$ keV) were produced with the gas ion source that is directly connected to the desorption facility. The ECR-ion source was used when higher energy beams ($3.0 - 10.0$ keV) were needed. All the irradiations in these measurements were done at room temperature. Heating cycles were linear from the room temperature up to 900 K. The sample was sputtered with argon and heated up to 1000 K between measurements for removing impurities.

Up to five different peaks were obtained in a helium desorption spectrum. Peak temperatures are roughly 300 K, 400 K, 550 K, 700 K and 800 K (Figure 3.1). First two peaks are present almost in all measured spectra. All other peaks are more

strongly dependent on the irradiation doses and energies. At lower irradiation energies and doses there is clear threshold energy after which the peaks appear. In our measurements this threshold energy seems to be around 0.5 keV. When the doses are lower than 10^{13} $ions/cm^2$ and the energy is below the threshold value, only one peak is seen around 400 K. When the dose increases to 10^{14} $ions/cm^2$ another peak appears at the temperature of 550 K. Measured spectra with low irradiation energies is shown in figure 3.1.

When the dose is larger than 10^{12} $ions/cm^2$ and the energy is increased to 0.5 keV or above, three peaks is seen in the spectra. The last two peaks, labeled as G and H, are seen at higher irradiation energies, too. The only peak that can be clearly described with first order kinetics is the peak that is labeled as H. This can be deduced from the shape and from the half-width of the peak. All the other peaks are either too wide or too symmetric with respect to the peak maximum. It is possible that these peaks are combinations of two peaks that are overlapping.

The intensity of the H peak increases rapidly when the dose is increased. When the irradiation energy is increased the intensity of this peak increases only slightly once the beam energy is above the threshold value. When these observations are combined with the fact that the most common defect that is created in a low energy irradiation is a vacancy-interstitial pair, it can be stated that the H peak is due to the helium release from monovacancies. Peak analysis with the methods described in section 4, gives an activation energy of 2.0 eV to the H peak. The determined activation energy for the helium dissociation from a monovacancy is in perfect agreement with the theoretical calculations[27], described in the section 5.

The first peak that is seen at the temperature of 300 K is probably due to the release of interstitial helium atoms or helium atoms that are weakly trapped at vacancies within the first few surface layers. The intensity of this peak is usually high and the peak is present in every spectrum. In fact, this peak is seen already at lower temperatures if the sample is cooled down before the ion implantation is done.

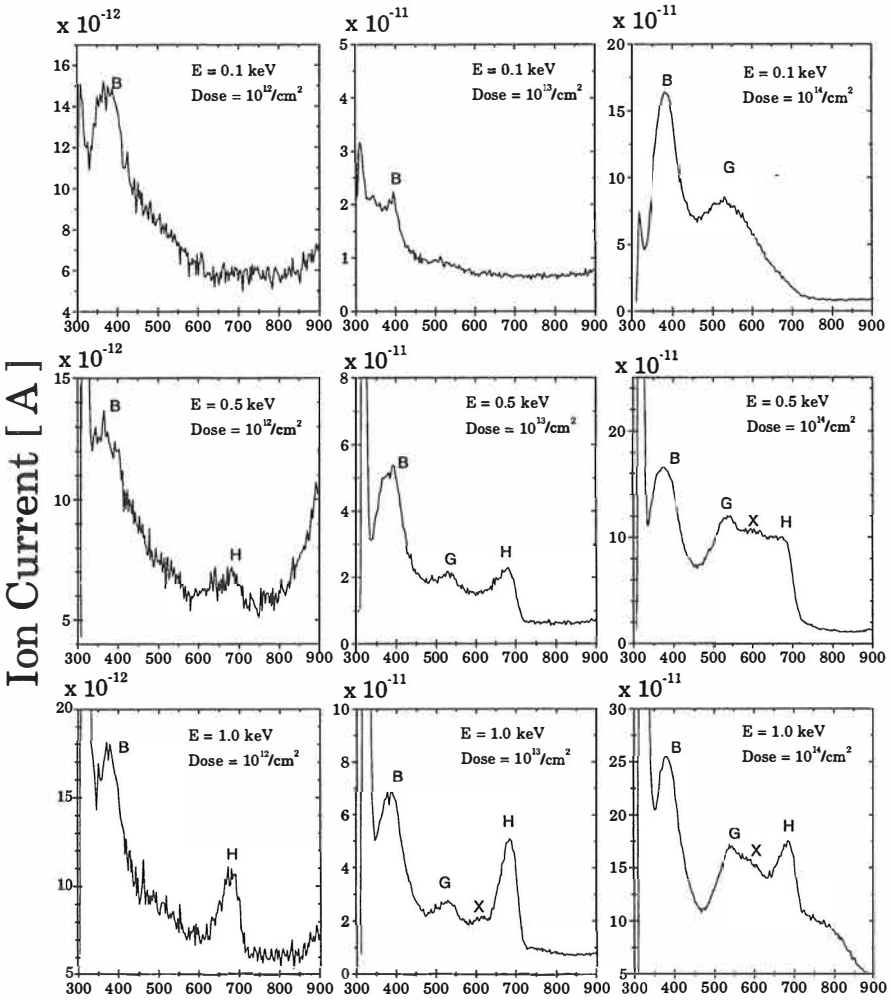

Figure 3.1. *Measured thermal helium desorption from copper. Irradiation energies were* $0.1 - 1.0$ *keV. Beam incoming angle was* $30°$ *with respect to surface normal.*

Possible explanations of the G and X peaks are a monovacancy filled with two helium atoms and a divacancy filled with one helium atom. These peaks were studied more carefully with annealing experiments, where the sample was annealed

at 400 K and at 500 K, before the actual desorption measurement was done. This annealing procedure gives spectra which show only the peaks that appear at higher temperatures than the annealing temperature. The irradiation energy was 1 keV and the dose was in the range of $10^{13} - 10^{14}$ $ions/cm^2$. Measurements were repeated with the helium post-implantation, i.e. the sample was bombarded with 0.1 keV helium beam after the high energy irradiation. The measurements show that the G peak is strongly dependent on the dose since the peak intensity increases rapidly when the dose increases. The peak is not visible at low doses. The half-width of the peak increases as well as intensity when dose increases. Earlier measurements showed that this peak is dependent on the irradiation energy, too. However, the dependence on the energy is not so strong as the dependence on the dose. This behavior indicates that the G peak is associated to multiple filling of a monovacancy. There might be also other effect combined with this since the peak becomes very broad when the dose is increased to 10^{14} $ions/cm^2$. Since the width and the shape of peak are different from those expected from first order kinetics, various peak analysing methods should be used carefully. The easiest way to estimate the activation energy is to assume that vibration frequency is the same as for the H peak, $\nu = 10^{13}$ $1/s$ (see section 4). This estimation gives an activation energy of 1.52 eV for the G peak.

Another peak that is dependent on the dose is the peak labeled with X. This peak is seen already at low doses, but increasing the dose increases the peak intensity slightly. The X peak is however more strongly dependent on the irradiation energy and the peak is seen only when the energy is above 3.0 keV. This is a clear hint that this peak is related to divacancies. The dose dependence is not so strong as expected in the case of multiple filling, so the only reasonable explanation of this peak is helium atom releasing from a divacancy. Other authors have proposed also alternative processes that could explain the X peak [27]. It is not completely ruled out that the peak could be caused by helium atom releasing from the divacancy which is doubly filled. Determination of the activation energy is again somewhat complicated but if we assume again that the vibration frequency is 10^{13} $1/s$ we get an activation energy of 1.73 eV for X peak.

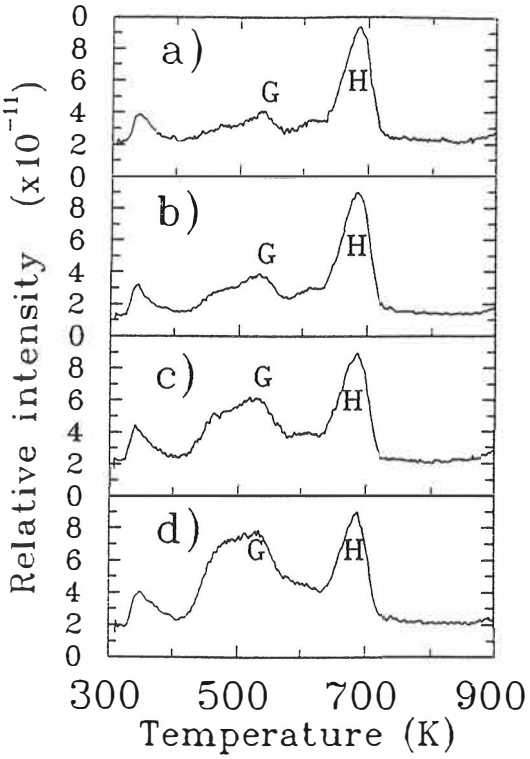

Figure 3.2. *Helium desorption from copper. Before the actual measurement, the sample was annealed some time at 400 K. Post irradiation doses are a) none b)* 10^{13} *ions/cm*^{2} *c)* $3 \cdot 10^{13}$ *ions/cm*^{2} *and d)* 10^{14} *ions/cm*^{2} [6].

A few helium desorption spectra were recorded so that the sample was cooled down to 200 K or below before the irradiation was done. The same doses and energies were used as in earlier measurements. These low temperature irradiations show strong X and H peaks. Intensities of these peaks are increased by a factor of ten when compared to the room temperature bombardments. This can be explained with the fact that at room temperature helium atoms are mobile and a large fraction

of them migrates to the surface and escapes from the sample during irradiation. When the sample is cooled the migration of helium atoms is not favored and the trapping at vacancies is more efficient.

Some attempts to measure diffusion was done during the cooling experiments. The sample was cooled down to $160 - 180\ K$ and irradiated with low doses. The desorption spectra were recorded as usual with the heating rate of $1.0\ K/s$. In some measurements we obtained a peak with a shape similar to that expected for a diffusion peak. The peak maximum temperature was at $180\ K$. However, when these experiments were done again with different heating rates it was obtained that the behavior of this peak is not consistent with a simple diffusion model. It might be that the temperatures reached with the cold finger were not low enough for diffusion measurements. Also impurities in the sample surface alter this peak readily. So no final conclusion could be made if this peak really represents diffusion. For more accurate measurements, lower temperatures and thinner samples are needed.

For comparison, some measurements were done by bombarding the sample with ^3He beam instead of ^4He. The energies and doses were similar for both isotopes. Basic features of the spectra were similar and same peaks were obtained in both cases. One difference in these spectra is that the measured ion current is larger for the ^3He and background level is higher. Higher background level is clearly due to inefficient pumping of the turbomolecular pump for the lighter elements, combined with the ^3He load from ECR ion source. The beam line of the ECR ion source is differentially pumped, but again turbomolecular pumps that are used are not very efficient for the light helium isotope and some amount of gas leaks to the vacuum chamber. The other effect, the increased intensity of the peaks, cannot be directly explained. It might be that one reason is a current density variation in the beam of ECR-ion source, although the measured doses are the same.

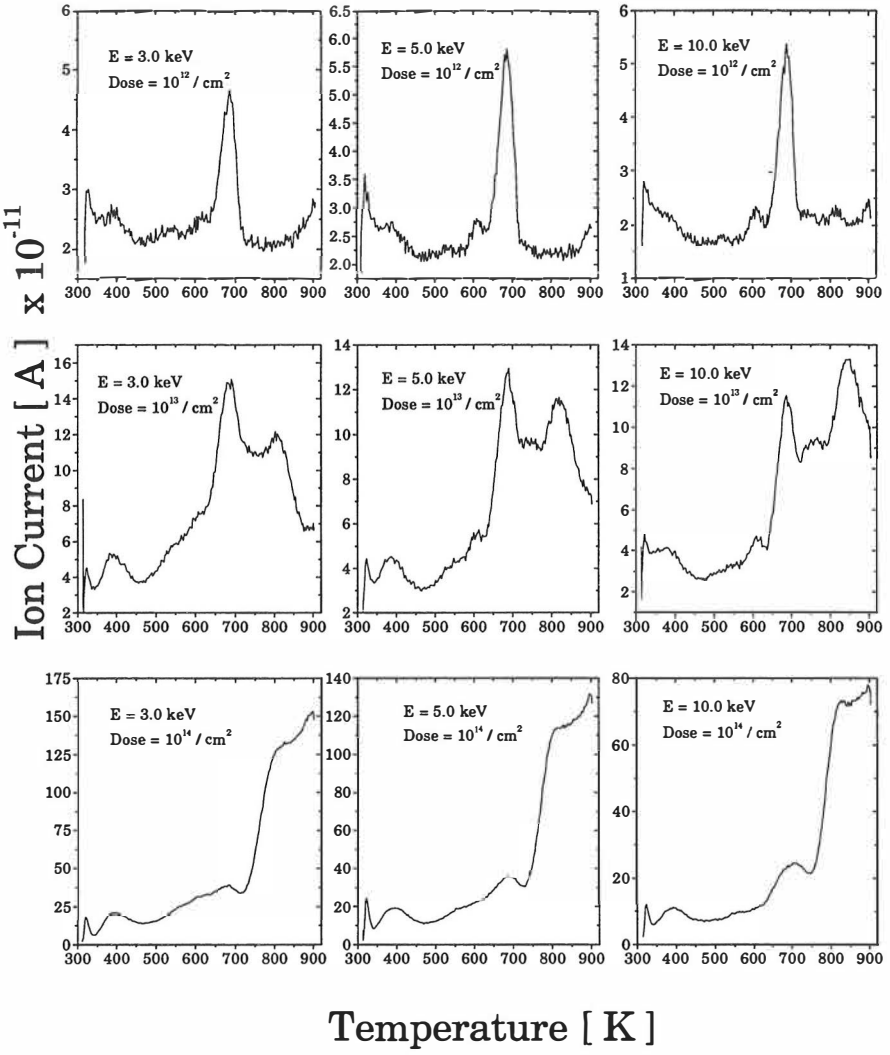

Figure 3.3. *Some helium desorption experiments were done with ^3He instead of the ^4He. Same peaks are present in both ^3He and in ^4He spectra.*

Although general features in the spectra are the same for both helium isotopes, one difference was found: the peak temperatures are 1–3 K lower for the lighter isotope. This is supposed to be due to the isotope effect. The classical activation energy is the same for both isotopes. However, due to different masses the frequency factors

will be different and with the harmonic oscillator model, some simple predictions can be made. The vibration frequency of an atom trapped at a harmonic potential well is inversely proportional to the mass and thus 15% higher for ^3He than for ^4He. If the peak positions are calculated from the first order kinetic equation by assuming that activation energies are the same, we get the result that peak position should be approximately 2 K lower for the ^3He. This conclusion is in fair agreement with the experimental observation.

3.2 Argon and neon desorption from copper

In the case of helium desorption clear peaks are observed and most peaks of the spectra can be explained. If neon or argon are implanted in copper, more complicated spectra are expected. For example, the penetration depths are lower and damage production capabilities are higher due to the larger size and due to the more efficient energy transfer to target. The lower mobility of heavier impurities and different relaxations of the host lattice around the impurity when compared to helium suggest that argon and neon desorption spectra show more peaks which are at higher temperatures than respective helium peaks.

In this work properties of neon and argon in copper were studied by bombarding the copper sample with neon and argon beams and performing the same heating procedures and desorption measurements as in the case of helium. The doses and incoming angles were similar than in helium measurements, $10^{12} - 10^{14}$ $ions/cm^2$ and $0° - 30°$, as well as the irradiation energies and the heating rate, $1.0 - 20.0$ keV and 1 K/s. The heavier atoms produce more vacancies which are distributed so that the maximum of the distribution is at lower depth than in the case of helium. For this reason, most of the measurements were done so that the sample was cooled down to 200 K when irradiations were done. This prevents vacancies from escaping to the surface during the bombardment. In some measurements, low energy helium was post-implanted at the same temperature.

Argon measurements show at least six different peaks when the bombarding energies and doses are low enough ($1.0 - 3.0\ KeV$ and $10^{12} - 10^{13}\ ions/cm^2$). Results are shown in figure 3.4. All the peaks are wider than usual first order peaks, but as mentioned earlier this may be due to peaks that are so close to each other that they overlap. Another reason for more complicated spectra is a high background level which may be caused by impurities trapped near the surface. When the energies and doses are increased, only two or three wide peaks are seen. This is clearly due to many different peaks that are partially overlapping. One striking feature in the argon spectra is the "double peak" with the peak maxima at the temperatures 485 K and 570 K. The same double peak is partially visible even when the doses are high ($10^{14}\ ions/cm^2$). The 570 K peak seems to be almost independent of the energy but increases with increasing dose. This is not the case for the 485 K peak, since it nearly disappears when the dose and especially the energy is increased.

Similar double peaks was obtained also in argon desorption measurements of nickel by Edwards [28]. In that case the peaks are at higher temperatures, but taking account the higher heating rates used by Edwards, we can say that the phenomena could have the same origin as in our case. Edwards proposes that one of these peaks are due to argon release from near-surface vacancies and the other from vacancies located deeper in the crystal. The main arguments for that prediction are the dose and energy dependences of the low temperature peak. In our case the low temperature peak nearly disappears when the energy is increased to $10-20\ keV$, but the dependence on the dose is weak. On the other hand the high temperature peak is nearly independent of the energy but its intensity increases with increasing dose. This fits quite well to the explanation presented by Edwards. We have presented also another explanation for these peaks (see paper IV). If the low temperature peak is due to the singly filled divacancy and the high temperature peak is due to a doubly filled divacancy the same arguments apply as well. It is natural to assume that the number multiple filled vacancies increases when irradiation dose increases.

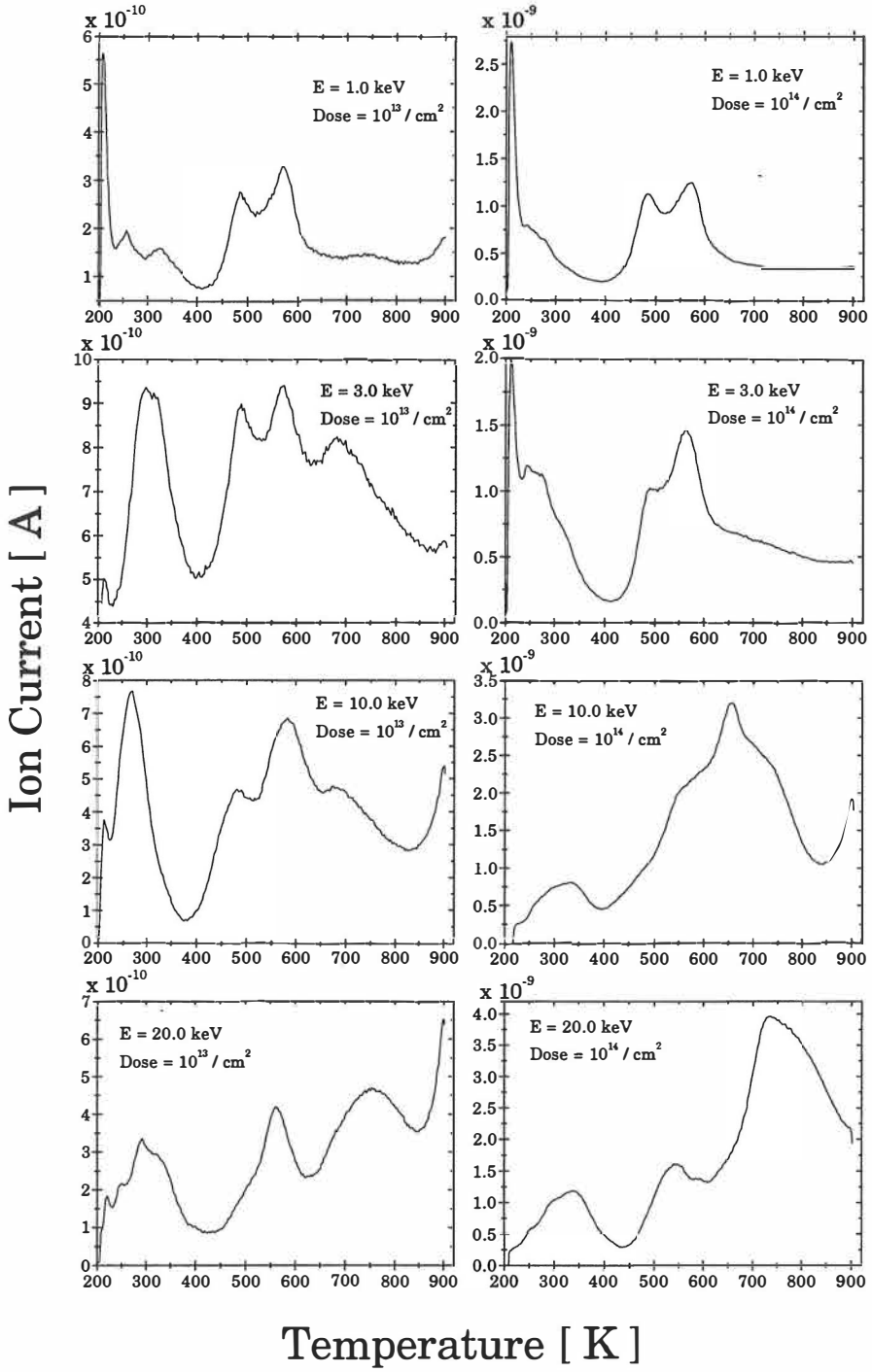

Figure 3.4. *Argon desorption from copper. Irradiation energies and doses used in these experiments are shown in the figure. Totally six different peaks are observed in argon desorption spectra.*

One problem with Edwards explanation is the energy needed to release an impurity atom from a monovacancy. In the case of helium, the peak that is due to helium release from a monovacancy is seen at around 700 K. In the argon spectrum the double peak is at a much lower temperature suggesting (according to Edwards) that heavier atoms are not so tightly trapped in a vacancy as a helium atom. This disagrees with theoretical calculations [27]. The question about the origin of the observed double peak is discussed in more detail in the chapter that describes results of theoretical calculations.

Neon measurements were done with similar doses and energies. The results are shown in Figure 3.5. These show the same general features that are seen in the argon spectra. The only exception is that the double peak is observed at higher temperatures. This would mean that a neon atom is more tightly trapped in a vacancy than the heavier argon atom. There are also some theoretical results that support this assumption: Bulk calculations give higher trapping and dissociation energies for the neon than for argon (paper II). However, the temperature of the peak is still too low to be purely due to neon atoms that are released from a monovacancy as explained above.

Another small difference is in the first peak, which seems to be much stronger for neon than argon. When the doses are low (10^{12} $ions/cm^2$) this first peak seems to consist of at least three overlapping peaks. The structure of the double peak is exactly the same as in the argon spectra and again the low temperature peak is more strongly dependent on the dose. The peak temperatures of the double peak are now 520 K and 660 K. These are clearly higher than the temperatures of respective argon peaks.

Before the desorption spectra of neon and argon can be explained more accurately theoretical calculations are needed. The calculations based on the effective medium theory are described in the chapter 5.

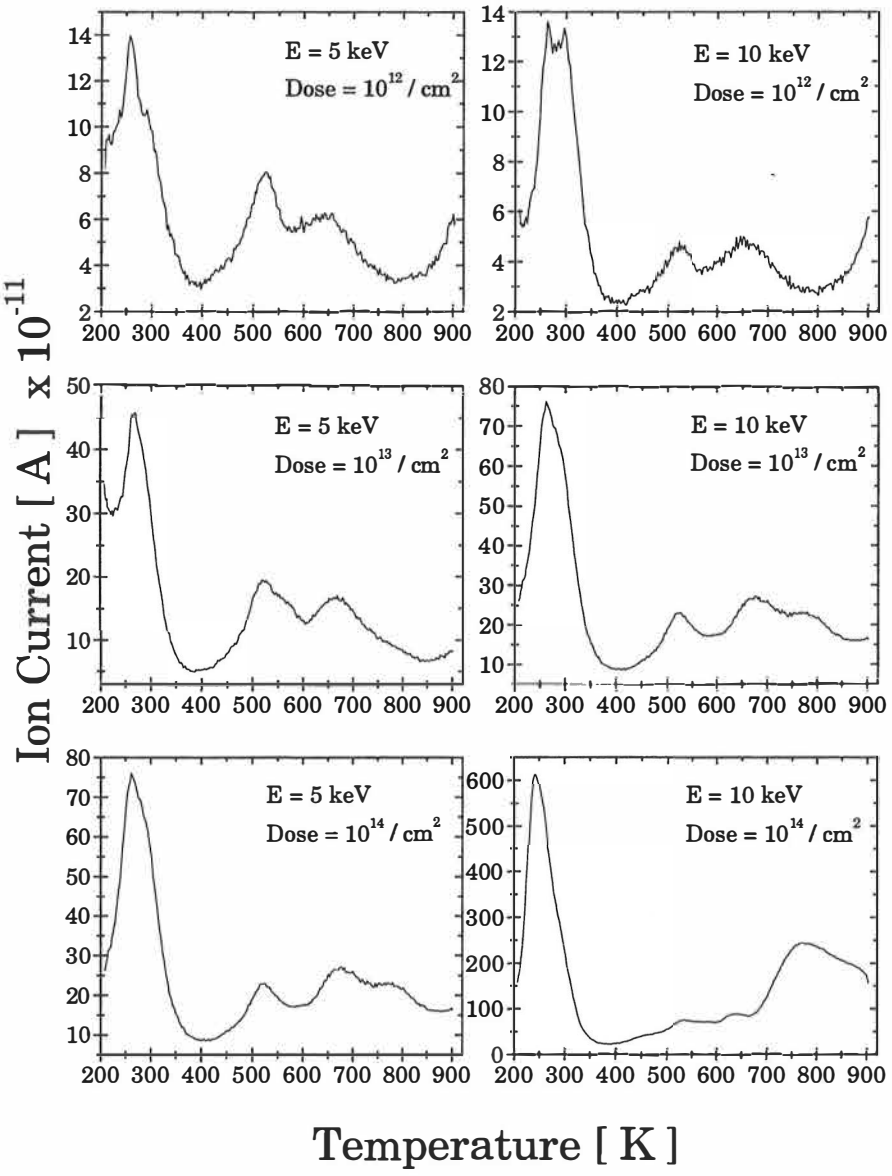

Figure 3.5. *Neon desorption from copper. Irradiation energies and doses used in these experiments are shown in the figure. Note the same double peak that appears in argon spectra.*

4. Analysis methods for desorption spectra

The first measurements using a thermal helium desorption spectrometer in University of Jyväskylä, were made during the year 1992. At this time the most usual method for the desorption peak analysing was the so-called Arrhenius line fitting method. This method is based on the fact that peaks shift toward higher temperatures when the heating rate increases. When enough measurements have been done with different heating rates, the activation energy and the frequency factor can be extracted from a fitted line [15]. We made hundreds of measurements and applied the Arrhenius method to the measured peaks. However, it was observed that results were quite dependent on the accuracy of temperature measurement [6,9]. Temperatures were measured with a thermocouple which has an accuracy of 0.5 – 2.0 K. This error can change the determined energy values by up to 40% and the corresponding error in the frequency factor can be 200%. Because of that we were forced to look for better analysing methods. It turned out that there are several methods that can be applied in peak analysis. During this work a few new methods for data-analysing were developed. All the methods are based on the kinetic equation introduced in the introduction and in paper III. In this chapter we briefly introduce the analysing methods and give some examples about the application of those methods [9].

4.1 Kinetic equations and the Arrhenius method

The kinetic equation describes the release rate of impurity atoms when the sample is heated [16,17]. As shown in the introduction it can be written as

$$R(T) = -\frac{dN}{dT} = \frac{\nu}{\mu}\,[N(T)]^m\, e^{-E_D/kT} \tag{4.1}$$

where μ is the heating rate (K/s), ν a frequency factor $(1/s)$, $N(T)$ the number of impurity atoms in the lattice in temperature T, m the order of the reaction, E the

activation energy for desorption and k the Boltzmann constant. When N is small or the impurity is a trapped rare-gas atom, the order of the reaction is usually one (m=1), since the reaction rate is proportional to the number of trapped atoms only (see section 1). Figure 4.1 shows examples how the peaks of different reaction order look.

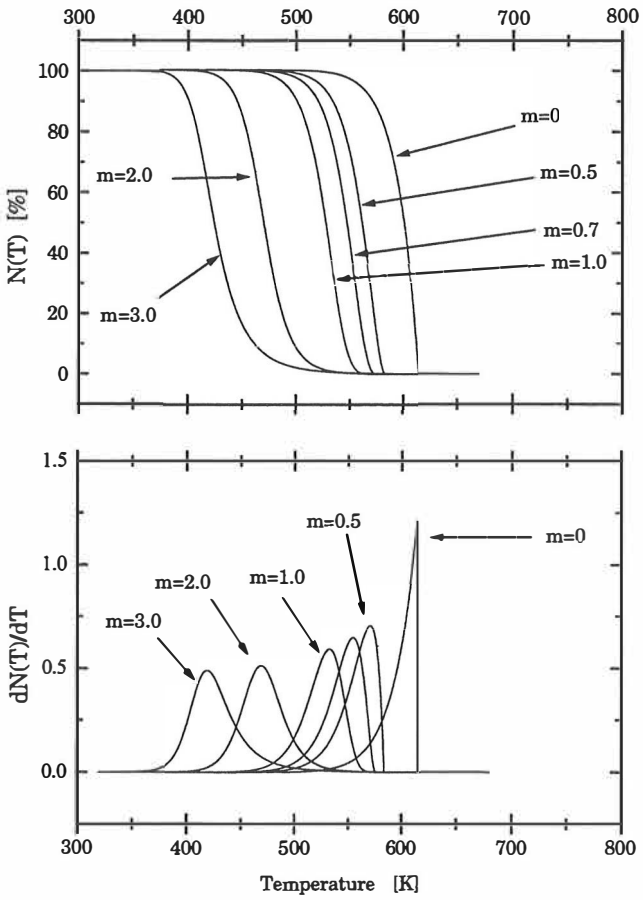

Figure 4.1. *Theoretically calculated desorption peaks with different reaction order m. Peaks are calculated from equation 4.1. In all cases activation energy is* $E_D = 1.5\ eV$, *frequency factor is* $\nu = 1.0 \cdot 10^{13}\ 1/s$ *and heating rate is* $\mu = 1.0\ K/s$.

The main parameters in the kinetic equation are the activation energy, the frequency factor and the heating rate. All these parameters together affect the shape and the position of the peaks. General trends can be seen in figure 4.2. When the heating rate increases, the peaks shift toward higher temperatures. This shift can be used to evaluate the activation energy for desorption. If several peaks are measured with different heating rates and the temperatures corresponding peak maxima are fitted according to

$$\ln\left(\frac{T_p^3}{\mu}\right) = \frac{E}{k}\frac{1}{T_p} + \ln\left[\frac{E}{m\nu k}\right] = A \cdot \frac{1}{T_p} + B, \quad (m \neq 1) \tag{4.2}$$

then the slope of the fit gives the activation energy and the constant term gives the frequency factor. When the order of the reaction is not one, the frequency factor must be determined carefully before this equation is applied. In the case of first order kinetics this reduces to a simpler form

$$\begin{aligned} \ln\left(\frac{T_p^2}{\mu}\right) &= \frac{E}{k}\frac{1}{T_p} + \ln\left[\frac{E}{\nu k}\right] = A \cdot \frac{1}{T_p} + B, \quad (m = 1) \\ \rightarrow E &= k \cdot A \\ \nu &= A \cdot e^{-B} \end{aligned} \tag{4.3}$$

This method for data-analysing is called Arrhenius line fitting method. It seems to be somewhat sensitive to errors in the temperature measurement as was mentioned before. Using this method needs a lot of measurements with wide variety of heating rates, since one measurement gives only one point in fitted line.

4.2 The Arrhenius method applied to a single peak

It was noticed that the Arrhenius method is also applicable in the case of only one measurement. First of all desorption rates can be normalized to one by dividing all rate values with the peak maximum rate value. In this case we can use current values measured with the mass spectrometer. The normalized rate is

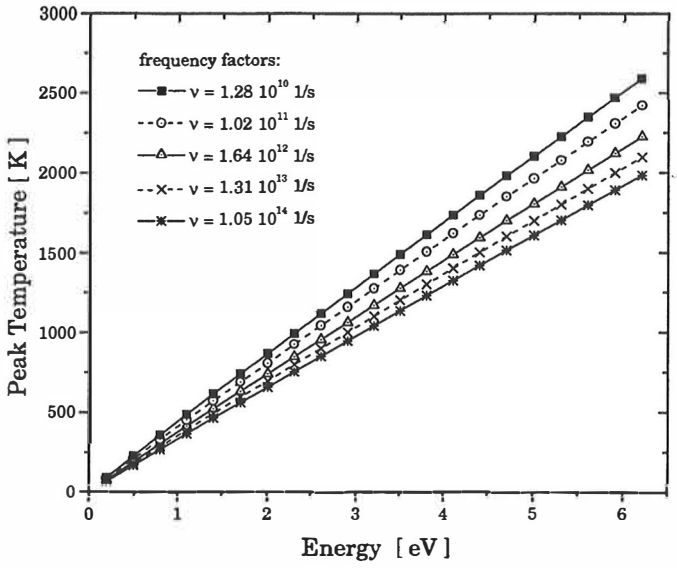

Figure 4.2. *Parameters that affect peak maximum temperature are energy, heating rate and the frequency factor. Figure shows the dependence of the peak temperature on the activation energy for a few fixed frequency factors in the case of first order kinetics.*

$$R_{norm} = \left[\frac{N(T)}{N(T_p)}\right]^m e^{\frac{E}{k}\left(\frac{1}{T_p}-\frac{1}{T}\right)} \tag{4.4}$$

Taking logarithm from both sides and rearranging terms we get

$$\begin{aligned}\ln(R_{norm}) =& m \ln\left[\frac{N(T)}{N(T_p)}\right] + \frac{E}{k}\left(\frac{1}{T_p}-\frac{1}{T}\right) \\ =& A \cdot \left(\frac{1}{T_p}-\frac{1}{T}\right) + B(T)\end{aligned} \tag{4.5}$$

This equation is not a linear since the constant term B is an unknown function of T. Fortunately the dependence is logarithmic which is slowly varying function. Another way to handle this problem is to solve E from equation (4.5)

$$E = k\left(\frac{T_p T}{T-T_p}\right)\left[\ln(R_{norm}) - m\ln\left(\frac{N(T)}{N(T_p)}\right)\right] \tag{4.6}$$

Now the last term contains unknown function $N(T)$. We can however integrate the peak area to get $N(T)/N(T_p)$. The equation is not continuous when the temperature equals the peak maximum temperature. Corresponding datapoint cannot be used in the peak analysis. This equation contains two logarithm terms which are not sensitive to errors in the argument and also the temperature dependent prefactor is not so sensitive. We can argue that this method should give quite good results when applied to peak analysing.

4.3 The peak area method

The peak area method was developed by the author of this thesis [9,18]. This method is based on two respective areas of one peak. It can be derived from the kinetic equation which represents one peak in the spectrum. If there is a peak in the spectrum, there must be two points where desorption rates are equal, $R_n(T_1) = R_n(T_2)$, and the temperatures T_1 and T_2 are such that $T_1 < T_p < T_2$. At these temperatures we can set the right sides of the kinetic equation equal. By dividing both sides of this equation with (ν/μ) and with $N(T_2)^m \exp(-E/kT_1)$ we get

$$\left[\frac{N(T_1)}{N(T_2)}\right]^m = e^{-\frac{E}{k}\left(\frac{1}{T_2}-\frac{1}{T_1}\right)} \tag{4.7}$$

The next step is to take logarithm of both sides and rearrange the terms

$$E = mk\left(\frac{T_1 T_2}{T_2 - T_1}\right)\ln\left[\frac{N(T_1)}{N(T_2)}\right] \tag{4.8}$$

In this equation there is again a singularity when T_1 equals T_2. This discontinuous point is the peak maximum point $T_1 = T_2 = T_p$, meaning that the peak maximum point cannot be used when we use this method for peak analysing. This equation contains again the number of atoms present in the lattice at temperatures T_1 and T_2. Absolute values for these are not known since the mass spectrometer measures ion current as a function of the temperature. However, if we integrate two partial areas of peaks these integrals should represent values for $N(T_1)$ and $N(T_2)$ and dividing these two areas we get exact result for $N(T_1)/N(T_2)$. This means that the

peak area method is accurate because we have not done any further simplifications in these equations. Also statistical errors are small because there are usually 30–60 data points which can be used. The number of the data points is dependent on the heating rate and when the heating rate is slow there are more data points which can be used. So this method prefers small heating rates.

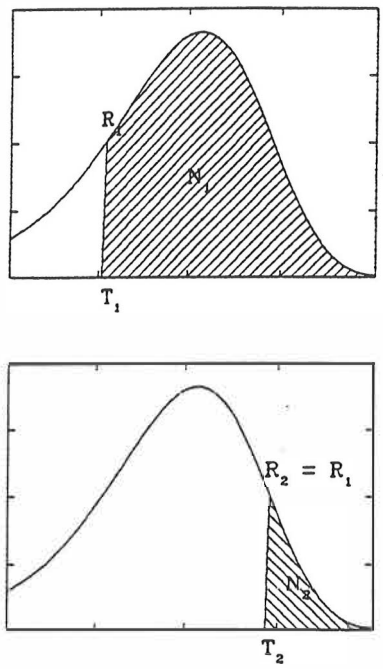

Figure 4.3. *Determination of the partial peak areas when using peak-area method in activation energy determination* [9].

We have tested this method with large amount of peaks. These tests have shown that the accuracy of this method is not drastically dependent on errors in the temperature measurement. This is the main point of this method. However this method is not so useful when there are overlapping peaks in the spectrum, since then peak areas can not be integrated.

4.4 Numerical integration and peak fitting to a theoretical shape

The author of this thesis developed this method independently, although later it turned out that ideas about the theoretical peak integration was presented earlier, however not in this particular form. This peak analysing method is based on numerical integration and fitting of measured data to the theoretical peak shape. If we integrate both sides of kinetic equation we obtain [18]

$$N_0^{1-m} - N(T)^{1-m} = -\frac{\nu}{\mu}\cdot(1-m)\int_{T_0}^{T} e^{-E/kT}dT \qquad (m \neq 1)$$

$$\ln\left[\frac{N(T)}{N_0}\right] = -\frac{\nu}{\mu}\int_{T_0}^{T} e^{-E/kT}dT \qquad (m = 1) \qquad (4.9)$$

The unknown constant ν/μ can be eliminated by using the condition for peak maximum

$$-\frac{E}{kT_p^2} = \frac{m\nu}{\mu}N(T_p)^{1-m}e^{-E/kT_p}, \qquad (m \neq 1)$$

$$-\frac{E}{kT_p^2} = \frac{\nu}{\mu}e^{-E/kT_p}, \qquad (m = 1) \qquad (4.10)$$

The number of atoms present in lattice at temperature T can then be written as

$$N(T) = \left[N_0^{1-m} + \frac{E(m-1)}{mkT_p^2}e^{E_D/kT_p}N(T_p)^{m-1}\int_{T_0}^{T} e^{-E_D/kT}dT\right]^{\frac{1}{1-m}} \qquad (m \neq 1)$$

$$N(T) = N_0 \exp\left[\frac{E}{kT_p^2}e^{E/kT_p}\int_{T_0}^{T} e^{-E/kT}\right] \qquad (m = 1) \quad (4.11)$$

If we substitute these functions for N back to rate equation and use the condition for peak maximum again we get following results for desorption rate equations

$$R_n = \left(\frac{-E}{kT_p^2} e^{E/kT_p} \frac{1}{N(T_p)^{m-1}}\right) \left[N_0^{1-m} + \frac{E(m-1)}{mkT_p^2} e^{E/kT_p} N(T_p)^{1-m} \int_{T_0}^{T} e^{-E/kT} dT\right]^{\frac{m}{1-m}} e^{-E/kT}$$

$$R_n = \left(\frac{-E}{kT_p^2} e^{E/kT_p}\right) N_0 \exp\left[\frac{E}{kT_p^2 e^{E/kT_p} \int_{T_0}^{T} e^{-E/kT} dT}\right] e^{-E/kT} \qquad (4.12)$$

If we now normalize these rate equations by dividing the rates with respective maximum values ($T = T_p$) we get equations with only one unknown constant E. Next we take the normalized rates from measured data and iterate the energy values that solve these equations. The steps needed for peak analysis in this method can be summarized as

1. Subtract possible background intensity from measured data.
2. Normalize measured current values by dividing these with the maximum value. This gives normalized desorption rates, (R_{norm}), in one peak.
3. Substitute these normalized rate values to equations above and iterate the energy value from these equations. Do not use the peak maximum value because it is a singular point. Every other measured rate value gives one estimate for the energy.
4. Calculate the mean value for the energy and substitute this back to the peak maximum condition. This gives an estimate for the frequency factor.

In this procedure, numerical integration and energy iteration can be done as accurately as needed. Also statistical errors should be small. However, accuracy of the temperature measurement is again important because this equation is somewhat sensitive to the noise of the signal. This sensitivity can be avoided if the measured data is smoothed before analysing. The smoothing can be done with the moving mean value method or with the peak fitting procedure. We have tested this method also with a large variety of measurements and it seems that it produces almost the same energy values as the peak area method gives.

4.5 The FWHM method

The idea of using the peak half width in peak analysis is not new. Chen introduced this kind of method already twenty years ago [40]. However we constructed our own method, which is based on relations between the half width of full maximum and the peak maximum temperature for the reaction order one [6]. We noticed that the term which contains the half width of the peak, the peak maximum temperature and the activation energy is a linear function of the ratio of the peak maximum temperature and the energy

$$\frac{T_p^2}{\Delta_{1/2}E} = a + b\frac{T_p}{E} \tag{4.13}$$

By calculating theoretical peak shapes and temperatures we obtain parameters for this equation and can solve the activation energy. For the reaction order one the parameters are

$$\begin{aligned} a &= (4751.2 \pm 0.4) \\ b &= (0.5314 \pm 0.0009) \end{aligned} \tag{4.14}$$

giving

$$E = 2.1047 \cdot 10^{-4}\frac{T_p^2}{\Delta_{1/2}} - 1.1184 \cdot 10^{-4}T_p \tag{4.15}$$

This method is not ideal one but it gives the first estimate of the activation energy with a little effort and the method is not drastically dependent on the accuracy of the temperature measurement [6,9]. The main point in this scheme is that no computer handling of the data is needed, but the values can be calculated directly from the peak maximum temperature and half width of the spectrum. It is also possible to include a quadratic term, which yields even better results [6]. This method is very useful, if first hand estimation is needed for example when the least squares method is applied to peak analysing. In practice, there may be some difficulties when determining the half-width if the background level is high.

4.6 The general case and nonlinear least-squares fitting

The most common analysis method is the least-squares fitting. In this scheme the square sum of the difference between the measured data and a theoretical function is minimized using various methods. This is the method of choice when the reaction order in kinetic equation is not known exactly, since the fitting can give this parameter too. This method has been proposed and used by many authors [19]. We have implemented and tested this method with a large set of measured spectra. It seems that this method yields reasonable results when the peaks can be separated so that at least top 10 – 15% of the peaks are not overlapping. In practice, results obtained with the least squares fitting are not better than corresponding values from other methods. In some cases the peak fitting gives clearly too high reaction orders. This is obtained particularly if a wide peak actually consists of two separate but overlapping peaks. This is natural, since in such a case, any of thc introduced methods can not be used properly.

4.7 Examples of the use of peak analysing methods

Before the peak analysing methods can be used, the reaction order must be known. In principle, when impurity atoms are released from lattice vacancies, the peak order should always be one, if the impurities do not form bonds with each other or with the lattice atoms. In the case of noble gases, this condition should be fulfilled. There are however peaks in the gas desorption spectra which are more or less symmetric and quite wide. These peaks usually consist of several overlapping and only look like one broad peak. In this case none of the peak analysing methods can be used to determine parameters. The only method that can give some estimations in this case is the nonlinear least-squares fit.

The only exceptions to the reaction order one in noble-gas desorption should be the case where atoms that are released from vacancies, are retrapped to existing vacancies while migrating towards the surface and the case where vacancy is filled

with two gas atoms. In former case the amount of detected gas atoms that are released depends on the number of vacancies as well as on the number of gas atoms that were originally trapped in the lattice. This process can be described with the second order rate equation. In practice all the peaks that are analyzed should be checked carefully, before it is assumed that reaction order is one.

There are only few approximate methods to find out what is the reaction order of a peak. By far the most simple method is just to look at the peak shape, and the half width. Figure 4.1 shows few theoretically calculated peaks with different reaction orders. As can be seen, the peak half-width increases when reaction order increases. This can be used as a first approximation in the peak order determination.

It would be useful to estimate, how large is the error if higher order peaks are analyzed as a first order peak. This can be done easily by calculating higher order peaks theoretically and applying peak analysing methods to them. When peak analysing methods that were developed to the first order reaction were used in peak analysing it was noted that the resulted energy was nearly 50% too low if reaction order was not correct. This yields even larger error to the frequency factor, since it is calculated from activation energy and from peak temperature. This show that peak order determination should be done carefully before analysing methods are applicable.

If the peak shape is similar than that of a first order peak, all the methods introduced above can be used directly. In this work new peak analysing methods were used mainly when helium desorption spectra were analyzed. In some cases these analysing methods were applied also to neon and argon desorption spectra. Helium spectra show usually few peaks that are clearly following the first order kinetics. Figure 4.4 shows peaks that were obtained in one measurement. Energies that are obtained with different peak analysing methods are also presented in the same figure. It seems that the Arrhenius method applied to one peak and the peak area method give almost the same results. Energies from the numerical integration and fitting method are slightly larger.

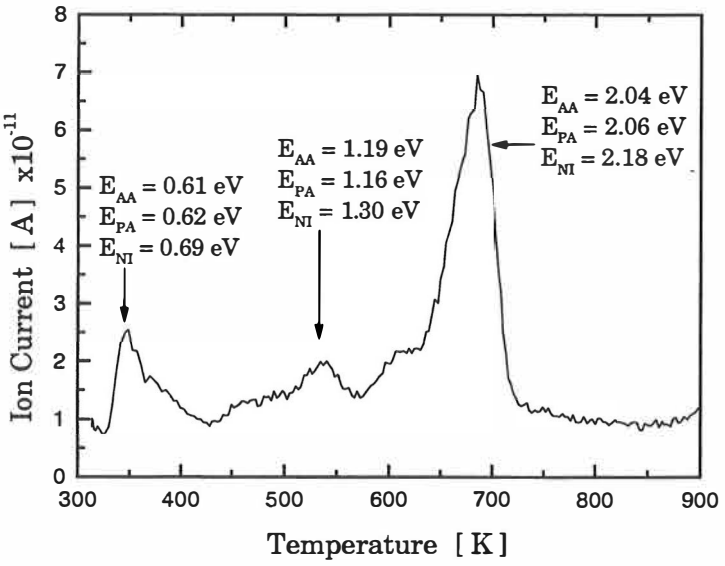

Figure 4.4. *Measured helium desorption spectra which show a few peaks and the activation energies calculated with different peak analysing methods. Subindex PA refers to peak-area method, AA to Arrhenius method which is applied to one peak and NI refers to numerical integration method.*

All introduced peak analysing methods, except half-width method, are so complex that the data handling and the peak-analysing has to be done with computers. In this work the peak analysing was done with a small program written with Visual Basic. Figure 4.5 show the main window of that program.

Due to the complexity of the peaks all analysing methods fail in some cases and the results they give can be very different. For that reason all the peaks should be analyzed at least with two independent methods. If these yield the same activation energies then it can be assumed that resulted energy is a good estimate to the true activation energy.

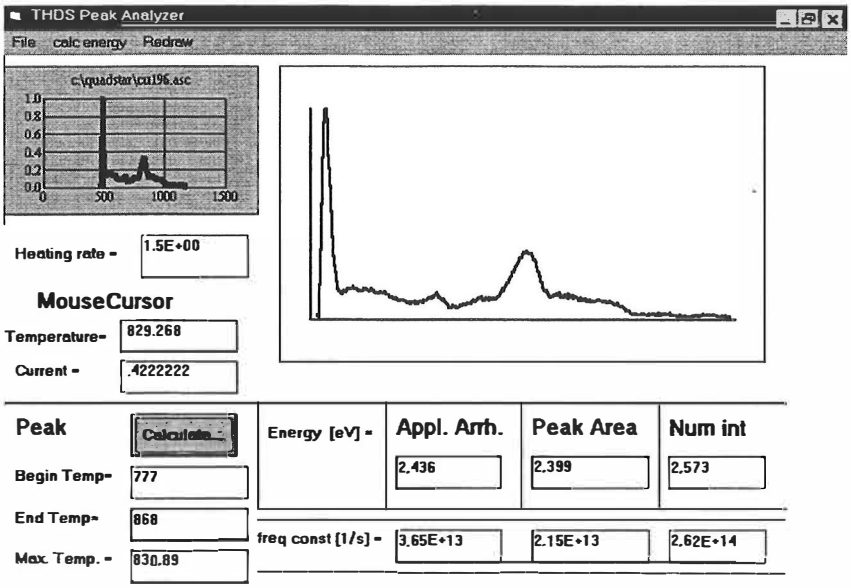

Figure 4.5. *Main window of the peak analysing program, done with Visual Basic. This program was used when desorption spectra was analyzed with peak-area method, numerical integration method and with Arrhenius method applied to one peak. Least squares fitting was done with another program due to the computational needs for that method.*

5. Effective-medium theory

During last years, there has been increasing amount of *ab initio* total energy calculations, which can describe chemical binding accurately within the density functional theory (DFT). The only approximation in these calculations is that the exchange-correlation energy is calculated locally by means of different interpolation formulas. The *ab initio* methods are suitable to systems which contain at most a few hundred particles, but not yet to cases where the system contains few thousand particles, like metal lattice with impurities. In this case something simpler is needed. One possibility is the effective-medium theory (EMT), which has been developed during last decade. It has been used in different studies which involve large structures and complicated geometries.

The basic idea in EMT is based on the changes in the electronic structure of an atom embedded in a homogeneous electron gas. This case can be solved accurately with the DFT using different LDA-approximations [32-37]. (In this work all the electronic structure calculations have been done with the exchange-correlation functional introduced in ref [37].) When embedding calculations are done with different jellium densities and the differences of the real metal lattice and this model host are approximated with a suitable model the results can be fitted to parametrized equations that can be used in total energy calculations. EMT is an *ab initio*-like scheme in the sense that no experimental parameters are used. Since electronic properties of atoms are calculated only once the system under study can be much larger than in Car-Parrinello type *ab initio* calculations.

In this work we have used a two-component EMT to calculate properties of noble gases in copper for finding out processes where these gas atoms are released from defects in the bulk metal.

5.1 Basic equations and approximations

The effective-medium theory has been explained in more detail in many papers [11-14], but a short introduction is anyhow given here. This introduction is based to the notations used in papers [11-12].

The theory is based on the energy of an atom embedded in a electron gas [12]. This is a reasonable starting point because in metals the atoms are screened by the local electron environment. The main contribution to the potential energy of an atom comes from the electron density provided by neighbour atoms.

The embedding energy of an atom in a homogeneous electron gas can be calculated within LDA. The only parameters needed are the density parameter r_s of the electron gas and the nuclear charge, Z, of the atom to be embedded. When an atom is embedded in an electron gas, its electron density changes due to the screening by the surrounding electrons. The induced electron density is usually denoted by $\Delta n(r) = n(r) - \bar{n}$, where $\bar{n}$ is the density of electron gas alone and $n(r)$ total electron density at site r when the atom is embedded. The total charge contained in the induced density is equal to $-e \cdot Z$ where Z is nuclear charge of embedded atom. We relate this embedding assumption to the real lattice situation in which all the atoms in lattice have been embedded to the same "electron gas" which at each atom site is formed by the density tails of the surrounding atoms. This density, seen by the atom in question, is thus a sum over the density tails of surrounding atoms

$$n(r) = \sum_i \Delta n_i(r - R_i) \tag{5.1}$$

Further simplification can be done by taking an average value of this density in the region of a neutral atomic sphere. When this averaging has been done the total energy of the atom i can be written as [12]

$$E_{Tot} = \sum_i E_{c,i}(\bar{n}_i) + \Delta E_{AS} + \Delta E_{1-el} \tag{5.2}$$

In the first term of this equation $E_{c,i}$ is the cohesive energy of atom i. It can be calculated as

$$E_{c,i} = E_{Hom,i}(\bar{n}_i) - \alpha_i(\bar{n})\bar{n} \tag{5.3}$$

where the first term is the embedding energy of the atom in a homogeneous electron gas of density $\bar{n}_i$. The second term describes the electrostatic attraction of electron density caused by neighbouring atoms. The quantity α is an integral over the neutral sphere of the induced potential ϕ which corresponds induced density $\Delta n(r)$,

$$\alpha = \int_{s(\bar{n})} 4\pi r^2 \phi(r) dr \tag{5.4}$$

The first correction term, ΔE_{AS}, in total energy function (equation 5.2) is the electrostatic repulsion of two nuclei when neutral spheres are overlapping each other. The last correction term tries to describe differences in one-electron energies (Kohn-Sham equations) between real metallic environment and homogeneous electron gas. However, this correction is very small when calculated for noble gases, and it can be neglected .

5.2 Two-component effective-medium theory

When the problem to be solved involves different elements, a special form of EMT is needed. This special form can describe chemical binding between different atomic species with the same approximations as described above.

The main part of the energy functional is the cohesive energy function, which is obtained by fitting the results of the embedding calculations to a third order polynomial [12]

$$E_c = E_0 + E_2 \left(\frac{\bar{n}}{n_0} - 1 \right)^2 + E_3 \left(\frac{\bar{n}}{n_0} - 1 \right)^3 \tag{5.5}$$

In this equation E_0, E_2 and E_3 are fitting constants, $\bar{n}$ is the density in which the atom is embedded and n_0 is the density where E_c-curve reaches minimum value. This fit is a good approximation as long as the electron density does not change too much from the density n_0 corresponding minimum cohesion energy. In the case of noble gases it is better to use a different approximation. This is due the fact that these atoms interact repulsively with any kind of atom and therefore the ideal density for a noble gas atom is zero. A suitable fit for rare gases is

$$E_c = E_1 \bar{n} + E_2 \bar{n}^2 + E_3 \bar{n}^3 \tag{5.6}$$

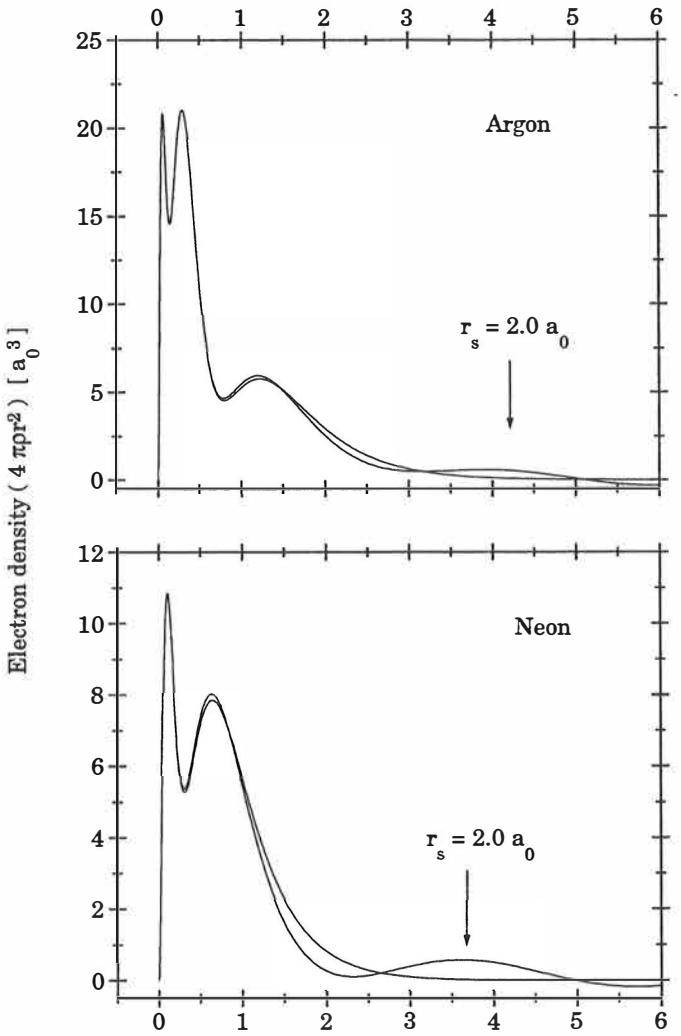

Figure 5.1. *Induced densities and free-atom densities for the argon and neon. Main differences between free atom and embedded atom are seen at distances* 2–6 a_0.

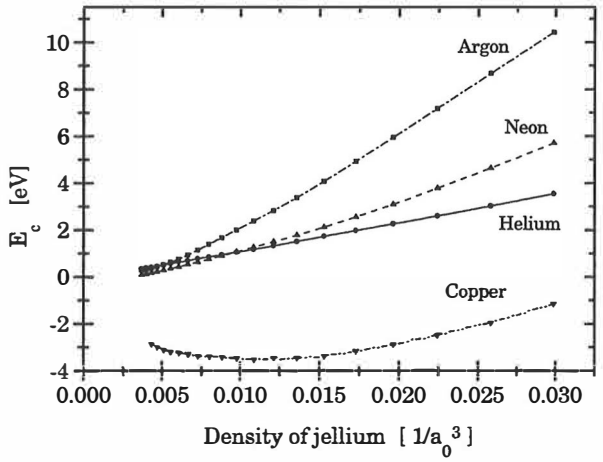

Figure 5.2. *Cohesion energy curves for helium, neon, argon and copper when they are embedded to electron gas as a function of density parameter r_s.*

The embedding density is usually approximated with an exponential dependence on the neutral radius s

$$\bar{n}(s) = n_0 e^{\eta(s-s_0)} \tag{5.7}$$

In this equation η is constant which describe the decay of the electron density of the atom and s_0 is the ideal neutral radius of the atom (a constant, which is just the neutral sphere radius when the background density is n_0). If only nearest neighbours are considered in an fcc-lattice, then the spherical average of density is assumed to be again of exponential form

$$\Delta\bar{n}(r,s) = \frac{n_0}{12} e^{\eta(s-s_0)-(r-\beta s_0)} \tag{5.8}$$

where $\beta = (2)^{-1/2}\left(\frac{16\pi}{3}\right)^{1/3}$ is the ratio of the WS-radius and the nearest neighbour distance in fcc-lattices and $\eta = \beta\eta_2 - \eta_1$. The next term in the total energy is the atomic sphere correction (second term in equation 5.2). When the atoms are

identical host atoms, this correction is [11]

$$\Delta E_{AS}^{MM} = \alpha \sum_i \left[\bar{n}_i - \frac{n_0}{12} \sum_{i \neq j} e^{-\eta(r_{ij}/\beta - s_0)} \right] \tag{5.9}$$

If the atoms are not identical i.e. they are a host metal-atom and an impurity atom, the atomic-sphere correction is described with the function

$$\Delta E_{AS,ik}^{AM} = V^{AM} \Omega_{ik}(r_{ik}) e^{-\phi_M^{AM} s_i - \phi_A^{AM} s_k - \phi_R^{AM} r_{ik}} \tag{5.10}$$

where $\Omega_{ik}(r_{ik})$ is the overlapping volume of two neutral atomic spheres, r_{ik} is the distance between the atoms, s_i and s_k are radii of neutral spheres of the host atom and the impurity atom and all other quantities are fitting constants.

When collected together we have six equations which must be solved for each atom in the total energy calculations [10,11]

$$\begin{aligned}
\bar{n}_i^{Cu} &= n_0^{Cu} \exp\left[-\eta^{Cu}(s_i - s_0^{Cu})\right] = \sum_{Cu} \frac{n_0^{Cu}}{12} \exp\left[\eta_1^{Cu}(s_i - s_0^{Cu}) - \eta_2^{Cu}(r_{ij} - \beta s_0^{Cu})\right] \\
\bar{n}_k^{I} &= n_0^{I} \exp\left[-\eta^{I}(s_k - s_0^{I})\right] \\
&= \sum_{Cu} \tilde{n}_0^{Cu} \exp\left[\tilde{\eta}_1^{Cu}(s_k - \tilde{s}_0^{Cu}) - \tilde{\eta}_2^{Cu}(r_{kj} - \tilde{r}_0)\right] + \sum_{I} \frac{n_0^{I}}{12} \exp\left[\eta_1^{I}(s_k - s_0^{I}) - \eta_2^{I}(r_{kl} - \beta s_0^{I})\right] \\
E_{c,i}^{Cu} &= E_0^{Cu} + E_2^{Cu} \left(\frac{\bar{n}_i^{Cu}}{n_0^{Cu}} - 1\right)^2 + E_3^{Cu} \left(\frac{\bar{n}_i^{Cu}}{n_0^{Cu}} - 1\right)^3 \\
E_{c,k}^{I} &= E_1 \bar{n} + E_2 \bar{n}^2 + E_3 \bar{n}^3 \\
\Delta E_{AS} &= \sum_{Cu} \left\{ \alpha^{Cu} \left(\bar{n}_i - \frac{n_0^{Cu}}{12} \sum_{Cu} \exp\left[-\eta(r_{ij}/\beta - s_0^{Cu})\right] \right) \right. \\
&\qquad \left. + \sum_{I} V^{I,Cu} \Omega_{ik} \exp\left[-\phi_{Cu} s_i - \phi_I s_k - \phi_R^{I,Cu} r_{ik}\right] \right\} \\
E_{Tot} &= \sum_{Cu} E_{c,i}^{Cu} + \sum_{I} E_{c,k}^{I} + \Delta E_{AS} \\
F &= -\nabla E_{Tot}
\end{aligned} \tag{5.11}$$

In the equations above, "I" refers to the trapped impurity and "Cu" refers to host-metal atom, which in our case is copper. The first equation gives the embedding density for the host-metal atom. In this case only the density coming from nearest neighbour metal atoms is included. This equation is also used when the neutral radius s_i for an atom is calculated because both sides of the equation are dependent on s_i. This means that the neutral radius must be solved iteratively from the density. The second equation gives the embedding density for the trapped noble-gas

atom. Now we include the density from the nearest-neighbour metal atoms and the density coming from other trapped impurities. Also in this case the neutral radius for the noble-gas atom must be solved by iteration, because both sides depend on s_k. When the embedding density and the neutral radius have been calculated for every atom, the cohesion energies can be calculated from the third and fourth equations. The fourth equation gives the cohesion energy for the noble-gas atom. The equation is different from that of a host atom, because the interaction is purely repulsive. According to this, the cohesion energy for a noble gas atom is positive, while the cohesion energy for a metal atom is negative. The fifth equation gives the atomic sphere correction coming from the overlap of neutral spheres. The first part is the atomic sphere correction for the metal-metal interaction and the second part gives the atomic sphere correction for the impurity-metal interaction. This term is important since it gives the main contribution to the interaction energy when neutral spheres are overlapping.

An analytical equation for the forces can be, in principle, calculated from these equations, but they are somewhat complicated, because the density and the neutral radius have to be solved iteratively. However, the forces can be calculated numerically once the energies have been calculated. This can be done by using difference equations. In this work, the difference equation that is used is

$$\frac{\partial E}{\partial x} = \frac{1}{12a}\left[E(x-2a) - 8E(x-a) + 8E(x+a) - E(x+2a)\right] \tag{5.12}$$

When these forces are calculated the atoms are finally moved according to equation of motion

$$d\vec{r} = \frac{d\vec{F}}{2m}(dt)^2 \tag{5.13}$$

where dt is time step and m the mass of the atom. When this equation is used, the time step must be sufficiently small. For example in case of a helium atom in a metal lattice, the time step should be approximately $10^{-16} - 10^{-15}$ s.

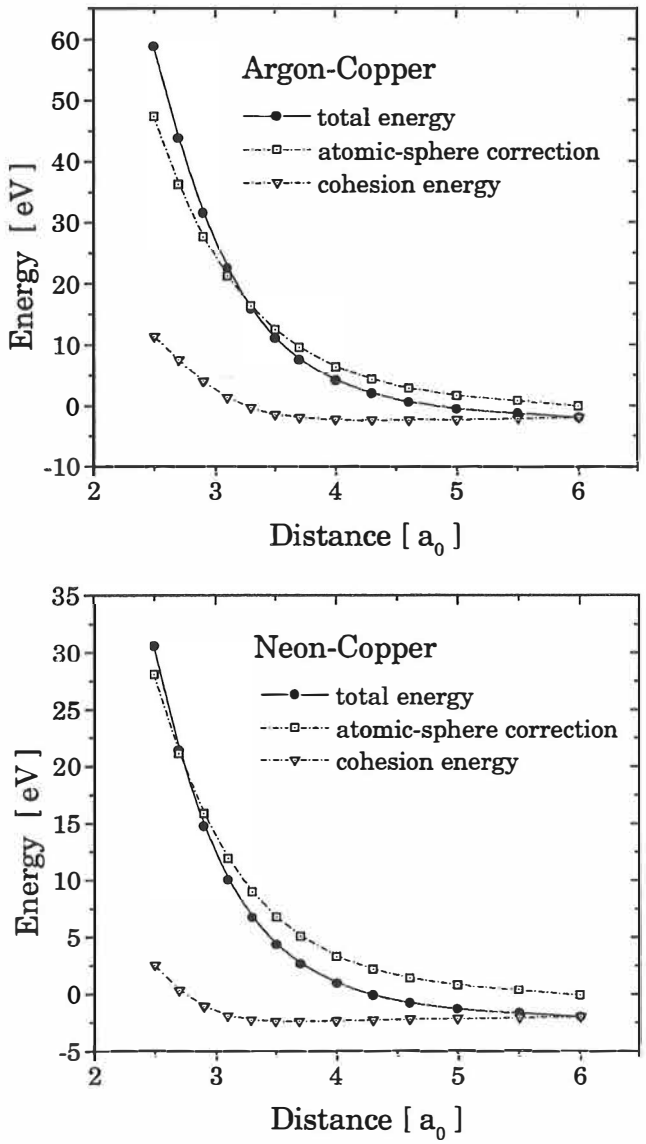

Figure 5.3. *Cohesion and atomic-sphere energies for argon-copper and neon-copper interactions according to the effective-medium theory. Note that the metal atom is not in a natural environment, but the Figure shows purely the pairwise interaction as a function of atomic distance. The atomic-sphere correction dominates when neutral spheres are overlapping.*

5.3 Parameters needed in two-component effective-medium theory

Parameters for pure materials have already been calculated for most of the elements using LDA [12]. Recently, for some elements the parameters have been calculated also with the generalized gradient approximation GGA [29]. However, in this work we use only the LDA parametrization. In the case of the two-component EMT additional parameters are needed. The first are the fitting parameters of the atomic-sphere correction for the impurity-metal interaction. The related energy, when two charge distributions are overlapping, is [11]

$$\Delta E_{AS}^{IM} = -\int_{overlap\ region} d^3r \left[\Delta n^M(r)\Delta\Phi^I(r) + \Delta n^I(r)\Delta\Phi^M(r)\right] \qquad (5.14)$$

where I stands for the impurity atom, M for the metal atom and Δn and $\Delta\phi$ are the induced density and the induced potential when the atom is embedded in a homogeneous electron gas. If these two quantities are taken from the embedding calculations, the integral can be directly calculated. This integration has to be done with different interatomic distances and with different induced densities, $\Delta n(r)$, corresponding to different values of the atomic-sphere radius. The integrals then give the overlapping energies as a function of neutral sphere radius of both atoms, s_i and s_k and as a function of distance between these atoms. These values can then be fitted with standard nonlinear least squares method to the form shown in equation 5.10.

Another set of extra parameters needed are $\bar{n}_0^{Cu}$, $\bar{\eta}_1^{Cu}$ and $\bar{\eta}_2^{Cu}$ (the third line in equation 5.11). These parameters determine the densities caused by nearest neighbours of different elements. They can be calculated from the induced densities with different distances and with different neutral sphere values. If we take the induced density values of the atoms and calculate a spherical average of the densities caused by other atoms inside the neutral sphere, we can calculate density values $\bar{n}_i^{Cu}$ and $\bar{n}_k^{Ads}$ in equation 5.11, as a function of distance and neutral sphere values for each atom. These values can then be fitted to exponential forms in equation 5.11. In these equations $\bar{r}_0$ (a center of the fit) should be selected so that it corresponds to

normal distances between these atoms, $s_0^{Cu,Ads}$ and $s_0^{Ads,Cu}$ are respective neutral sphere values corresponding to $\tilde{r}_0$. They should be near the pure material value s_0.

Parameter	Helium	Neon	Argon	Copper
E_0				-3.5620
E_1	98.8930	33.9120	44.6330	
E_2	1412.4	9153.2000	20375.0000	1.2870
E_3	-22747.0000	$-1.2787 \cdot 10^5$	$-3.3231 \cdot 10^5$	-0.2950
n_0	0.02095	0.02095	0.02095	0.01130
s_0	1.6459	2.0450	2.4500	2.5860
η	2.8760	3.4360	2.4150	2.4870
η_1	0.43600	0.42366	0.51830	0.23400

Table 5.1. *Pure material parameters of EMT for helium, neon and argon* [10].

Parameter	Helium	Neon	Argon
$\tilde{n}_0^{Cu}$	0.004391	0.004656	0.006902
$\tilde{n}_0^{Ads}$	0.001203	0.003334	0.007072
$\tilde{s}_0{}^{(Cu,Ads)}$	2.50	2.50	2.50
$\tilde{s}_0{}^{(Ads,cu)}$	1.60	2.00	2.40
$\tilde{\eta}_1{}^{Cu}$	0.439100	0.966530	0.979900
$\tilde{\eta}_2{}^{Cu}$	1.713900	1.890410	1.907700
$\tilde{\eta}_1{}^{Ads}$	0.818300	0.581640	0.589700
$\tilde{\eta}_2{}^{Ads}$	1.749500	1.746780	1.610950
$V^{(Ads,Cu)}$	284.8400	2070.1600	395.8769
$\phi_{Cu}^{(Ads,Cu)}$	0.6801	2.3347	1.4637
$\phi_{Ads}^{(Ads,Cu)}$	0.66950	1.79710	-0.01389
$\phi_R^{(Ads,Cu)}$	1.58190	0.32870	1.59480

Table 5.2 *Two-component parameters needed in EMT for helium, neon and argon in copper* [10].

5.4 Results for noble gases in bulk copper

Paper II describes calculations which were done for the case of noble gases in bulk copper. The main motivation for those calculations was the need to know migration energies, since there are only few experimental values that can be found in the literature for helium. Respective values for the argon and neon could not be found at all. Migration energies are important when peaks in thermal desorption spectra are analyzed, since delayed desorption due to the migration could shift the peak temperatures.

The first interesting result obtained in this work is the fact that the calculated migration energies for helium, $E_m = 0.5\ eV$, are the same for both octahedral-octahedral and tetrahedral-octahedral jumps (see figure 5.4). This is a surprise although helium is small and it does not disturb the lattice as much as heavier elements do. Although it is well known that helium is insoluble in lattices, this observation is new. As expected, the preferred interstitial site for helium in fcc lattice is the octahedral site. The tetrahedral site is also a local minimum but it is 0.4 eV higher in energy than the octahedral site and the trapping energy in tetrahedral site is only of the order of 0.1 eV. There is another local minimum exactly in the middle of two octahedral sites. The trapping energy, E_{He}^{B} (see figure 1.2), of this site is only 0.05 eV and it is likely that at finite temperature this minimum is wiped out by thermal vibrations.

Argon and neon are much heavier and larger than the helium atom. This suggest that the migration energies are much larger. When calculated with effective-medium theory, migration energies $E_M^{Ar} = 0.7\ eV$ and $E_M^{Ne} = 0.8\ eV$ were obtained. These are not as large as could be expected from the atomic sizes. It is a surprise that the migration energy of argon is lower than that of neon. This can be explained by comparing the η and V values of the EMT parameters. Both are larger for the neon. This is related to the different sizes of the atoms in metallic surrounding and to different tails of the induced densities. Overall shapes of the

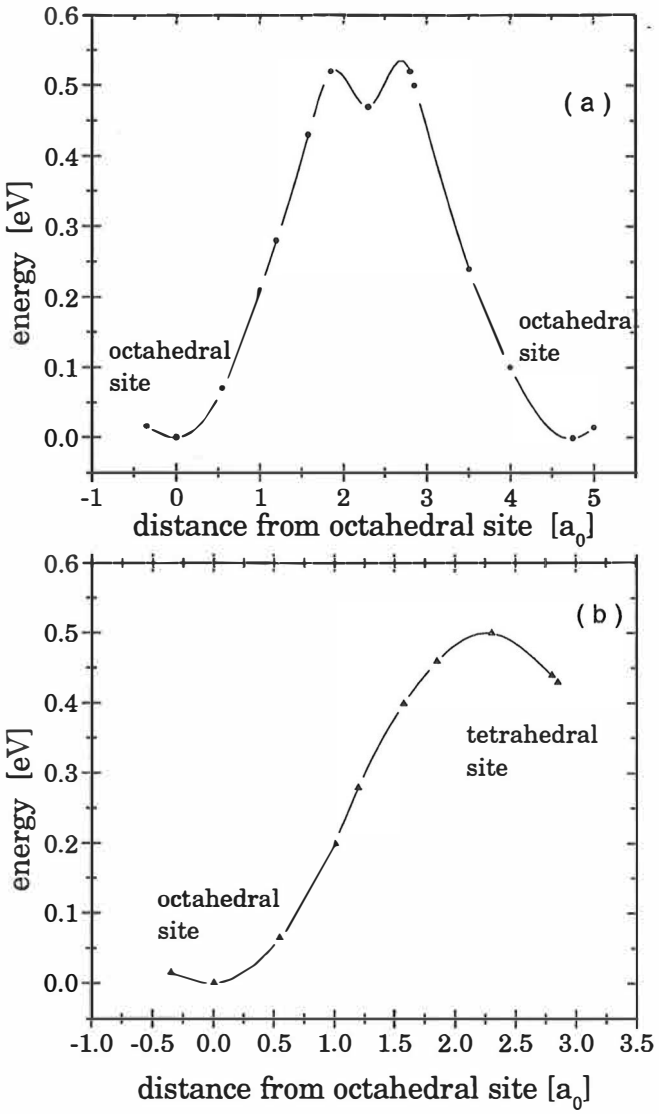

Figure 5.4. *Potentials for helium migration through octahedral and tetrahedral sites in copper. Height of the potential barrier is the same in both cases.*

potential energies along the migration are not similar for these two atoms (see figure 3. in paper II). The minimum energy site for neon is the octahedral site but for argon it is off-centered from the octahedral site. In case of the argon an off-centered tetrahedral site is also a local minimum, but it is much higher in energy than the off-centered octahedral site. In the case of neon there are no other local minima than the octahedral site. Due to these differences the preferred jump routes are different. For neon the migration seems to prefer octahedral-tetrahedral jumps but for argon the preferred migration route is octahedral-octahedral path.

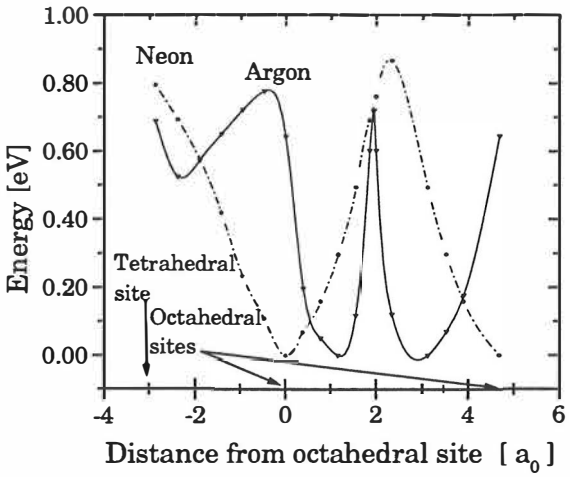

Figure 5.5. *Potentials for neon and argon migration jumps from octahedral to octahedral and from tetrahedral to octahedral site.*

Other interesting effects were observed when trapping and dissociation energies for the noble gases in vacancies were calculated. First of all, it was noted that the vacancy can be occupied with three helium atoms, two neon atoms but only one argon atom. These results were observed by occupying a vacancy with a few impurity atoms and making relaxation calculations. In these calculations all the atoms were mobile except the outer boundary layer of the lattice. If there are

more impurity atoms than the vacancy can occupy, the excess atoms are jumping quickly to the nearest interstitial sites and even further. In some other systems heavy impurity atoms can push the nearest metal atoms away from the lattice site and form a so-called dumbbel. In the case of neon and argon this was not observed, probably due to the highly repulsive interaction between the noble gas and the metal atoms. Minimum energy configurations for two and three helium atoms and for two neon atoms in a vacancy were highly symmetric and similar that are reported in other impurity-host systems [30,31]. Dissociation energies for those doubly and triply filled vacancies were 1.75 eV (two helium atoms in a vacancy), 1.45 eV (three helium atoms in a vacancy) and 1.90 eV (two neon in a vacancy). The helium values are in agreement with the experimental values. For the neon there are no experimental values available.

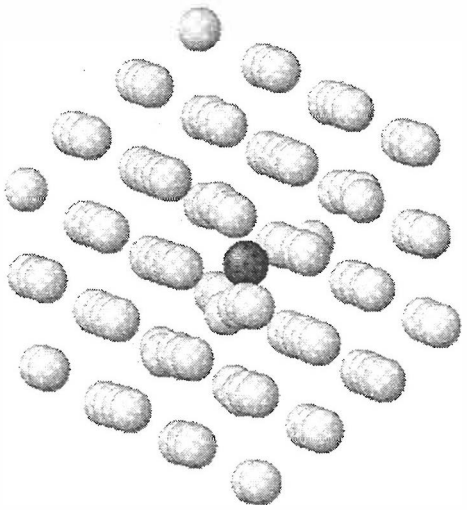

Figure 5.6. *Minimum energy site for argon in copper is off-centered octahedral site. Lattice relaxation around argon atom in minimum energy site is not fully symmetric.*

A surprising result was that in bulk copper neon atoms are trapped more strongly at vacancies than argon atoms. Again, this is related to the difference in the same EMT parameters as the difference in migration energies. Similar energy difference is obtained in thermal desorption experiments. The characteristic double peaks in argon spectra are at lower temperatures than the related peaks in neon spectra. It is however not possible to explain the origin of these peaks with the results of bulk calculations alone. In principle, it is possible that these peaks are related to desorption from layers that are near the surface, or the dissociation is assisted by mobile vacancies. The calculated energies for the helium, neon and argon dissociation from copper vacancy are given in the Table 5.3. In case of helium the result agrees well with the measured dissociation energy. For the neon and argon the dissociation energies are much higher. This suggests that the peaks especially in neon spectra are due to the desorption from different surface layers or the retrapping effect is important. In the case of argon and neon there are no experimental values available since the measured spectra are very complicated and can not be explained in detailed. No clear peaks are seen at temperatures corresponding to the calculated dissociation energies.

	Helium	Neon	Argon	copper
E_M (eV)	0.50	0.80	0.70	
E_B (eV)	1.67	3.00	2.18	
$E_{B,2}$ (eV)	1.19	-	-	
E_D (eV)	2.17	3.80	2.87	
$E_{D,2}$ (eV)	1.75	-	-	
$E_{D,3}$ (eV)	1.45	-	-	
E_V^F (eV)				1.45

Table 5.3. *Calculated energies to light noble gas migration, binding and dissociation in bulk copper. E_B is binding energy in vacant site, E_V^F is formation energy for vacancy, $E_{D,2}$ is dissociation energy of first atom when vacant site is filled with two impurity atoms.*

5.5 Neon and argon near the surface

Since the peaks in argon and neon spectra are very complex we extended previous calculations to different surfaces (paper V) and calculated the dissociation energies for the impurities trapped at different sites near the surface.

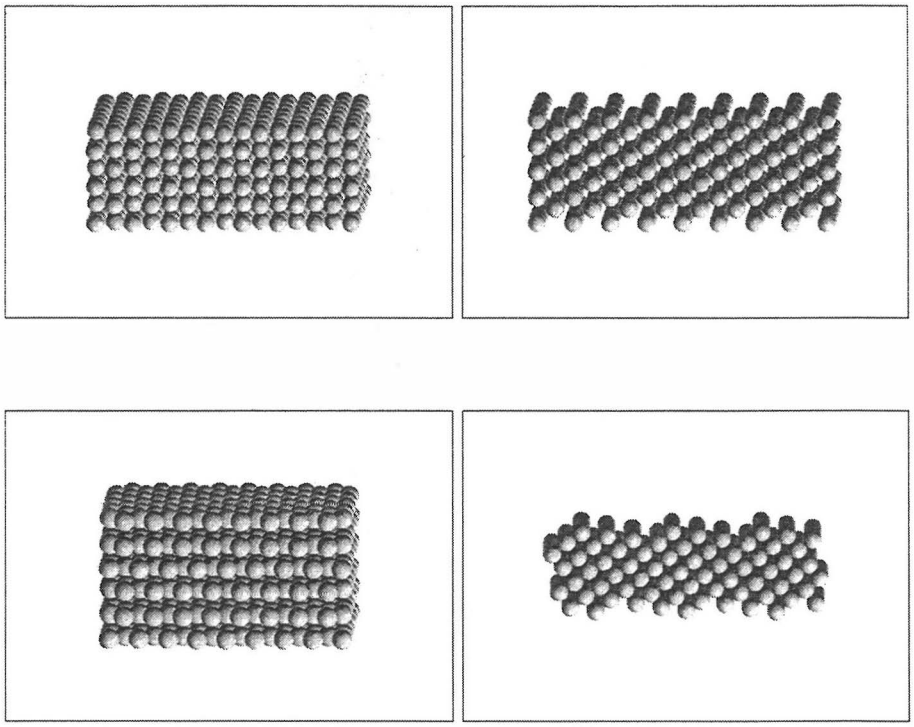

Figure 5.7 *Effective-medium-theory based calculations was done for different surfaces. First three surfaces are common low-index surfaces of fcc-metal (100) (upper left), (110) (upper right) and (111) (lower left) and last,(340)-surface (lower right), was selected since thermal desorption experiments were done with the sample which surface orientation was (340).*

Results are indeed different when compared to the bulk calculations. This is expected since surface relaxes more easily and trapping can be totally different. The calculations were done in a similar fashion as bulk calculations introduced above.

Four different surfaces were studied, in order to obtain differences in energetics when these impurities are desorbed from different sites and from different layers (figure 5.7).

The heat of solution is known to be relatively high for noble gases in metals. The energetics was calculated to all studied surfaces by moving impurity noble-gases with small steps from interstitial sites at bulk to surface through octahedral sites. At every step the atoms were allowed to relax freely to equilibrium sites. At every step, 2000-4000 time steps were needed for converged configuration. When the equilibrium structure was found the information was saved and the impurity atom was moved to the next position, etc.

Resulted energies for different surfaces were quite similar. Small differences in the energy barriers could be clearly explained with the packing density of the surface. The results are expressed in table 5.4.

In the cases of (100) and (111)-surfaces, the energies for the near surface migration seem to be similar due to the high packing density in both surfaces. In the case of argon these surfaces show a strong trapping site just under the surface.

Surface	ΔE_{neon} [$eV/atom$]	ΔE_{argon} [$eV/atom$]	surface relaxation [%]
(100)	6.40	9.37	-3.59
(110)	6.14	9.25	-2.63
(111)	6.23	9.64	-3.07
(120)	6.08	9.56	-2.63
(340)	6.03	9.60	-3.60

Table 5.4 *Energy barriers of solution for the neon and argon in different copper surfaces. Last column gives relaxation of the first atomic layer relative to ideal site. Inward relaxation is denoted by - sign.*

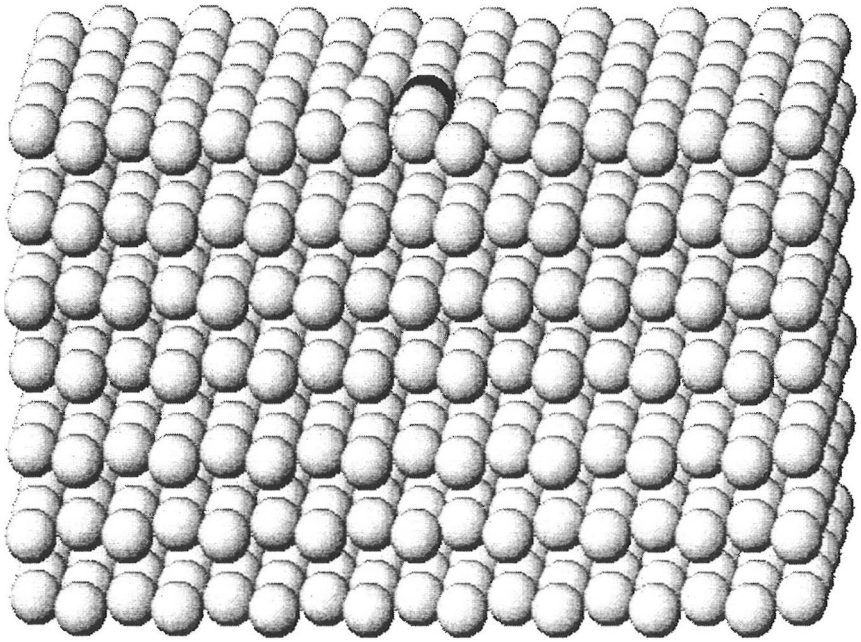

Figure 5.8. *Relaxation of the nearest atoms in (111)-surface when the argon atom is breaking through the surface via octahedral site. Argon atom is denoted by black color.*

The migration potential is lower for argon in both surfaces. The expected reason for that is the larger relaxation around argon atom in copper. Due to the larger relaxation the argon atom sees a more open channel for migration and the corresponding potential barrier is lower.

Migration barriers near the (110) and the (340)-surfaces are slightly different from the other two cases. This is due to the lower packing density in these surfaces which leads to stronger inward relaxation of the surface. In (110) there is a direct octahedral-octahedral channel. This changes migration barrier markedly. Now, there are several small minima in argon migration curve while the neon sees nearly

open channel for migration. In the neon case there is two weak trapping sites just under the surface.

The last surface studied, (340) is a stepped surface (see figure 5.7). This can be seen readily in the migration curve, since the region where the potential drops is now much larger than in the other surfaces. This is due to the geometry of the surface, since seven uppermost layers are in the step. The packing density of one atomic layer is small, but layers are near each other. This generates long ranged relaxation of surface layers.

More interesting than migration barriers are dissociation energies for the noble gas impurities trapped at vacancies or at some other defects near the surface. These energies can be compared readily with thermal desorption measurements. First dissociation energies for the impurities trapped in a monovacancy were calculated. Now the situation is more complicated than in the bulk, since relaxations are larger and less symmetric.

The simplest surface of copper fcc-lattice is (100). Neon or argon atoms at the surface vacancy are not bound at all. This is evident since the metal-noble gas interaction is fully repulsive. From the second layer on, neon and argon atoms are strongly trapped at vacancies. Calculated dissociation energies are 0.90 eV, 4.30 eV and 6.50 eV for the argon in the second layer vacancy, third layer vacancy and in the fourth layer vacancy, respectively. For neon the corresponding energies are 1.30 eV, 3.60 eV and 4.93 eV. The result for the third and fourth layer trapping are surprisingly high. This might be due to the surface relaxation since the density is higher in the relaxed surface region and the repulsion between metal and impurity atoms increases with increasing density. Qualitatively the potential barriers are similar for both of the impurity atoms.

The next surface that was studied was (110). In this surface impurities are trapped from the third layer on. Dissociation energies are only slightly lower than in the (100)-surface, although the packing density of the (100)-surface is somewhat higher. Dissociation energies for argon trapped in a vacancy are now $E_{Diss}^{Ar,V} = 3.3\ eV$

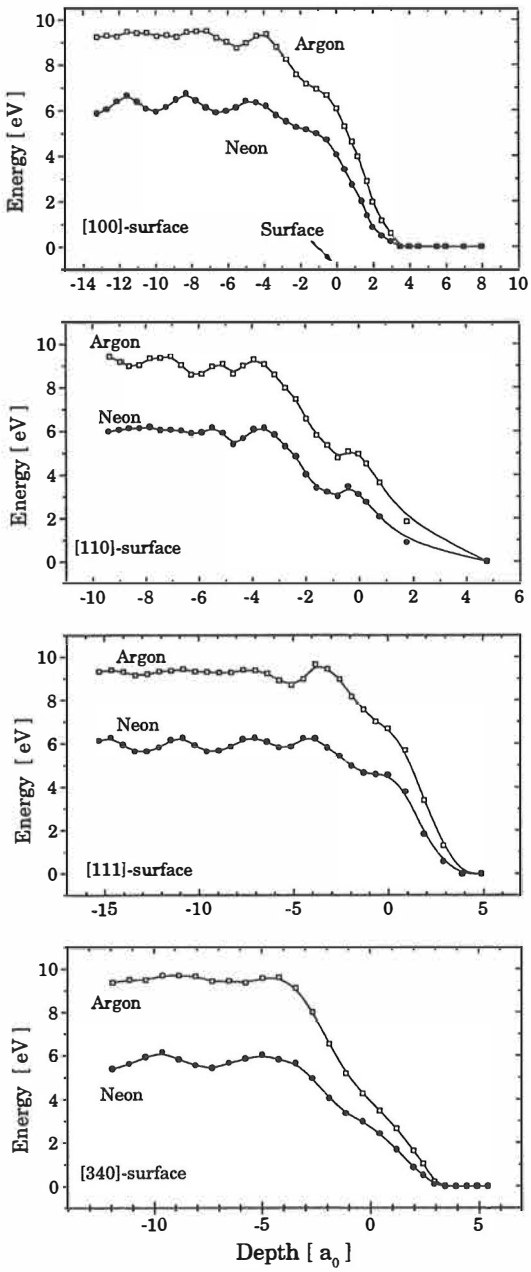

Figure 5.9. *Potential barriers for the near surface migration of argon and neon in copper and heat of solution in different surfaces. Energies are calculated with EMT by moving impurity atom from bulk to surface through interstitial sites with small steps.*

for the third layer vacancy and $E_{Diss.}^{Ar,V} = 5.38\ eV$ for the fourth layer vacancy. Neon is trapped already at the second layer vacancy, but the dissociation energy for that trapping site is only $E_{Diss.}^{Ne,V} = 0.06eV$. Dissociation energies for the gas atoms trapped in third and fourth layer vacancies are $E_{Diss.}^{Ne,V} = 2.93\ eV$ and $E_{Diss.}^{Ne,V} = 4.74\ eV$. For both of the impurities dissociation energies are again high.

In the (111)-surface the packing density is highest. This is seen readily in the dissociation potential barriers, since they are different when compared to other surfaces. Basic trends are still the same. Impurities are trapped if the vacancy is located in the second atomic layer or deeper. Dissociation energies are $E_{Diss.}^{Ar,V} = 2.90\ eV$, $E_{Diss.}^{Ar,V} = 5.99\ eV$ and $E_{Diss.}^{Ar,V} = 6.83\ eV$ for argon in the second, third and in fourth layer vacancy. Dissociation energies for neon are $E_{Diss.}^{Ne,V} = 3.00\ eV$, $E_{Diss.}^{Ne,V} = 4.75\ eV$ and $E_{Diss.}^{Ne,V} = 5.28\ eV$. One reason for the strong trapping is the outward relaxation of the vacancy, which increases the surface relaxation effect significantly. Figure 5.10 shows corresponding dissociation barriers for neon and argon trapped in near surface vacancies.

For the (340)-surface, dissociation energies in the immediate vicinity of the surface are smaller than respective energies for other surfaces. This is due to the step geometry of that surface. Impurity atoms are trapped if the vacancy is deeper than in seventh layer or the vacancy is below the edge of a step. Dissociation energies for the neon and argon trapped in 8:th and 9:th layer vacancies are $E_{Diss.}^{Ne,V} = 2.90\ eV$, $E_{Diss.}^{Ne,V} = 3.00\ eV$, $E_{Diss.}^{Ar,V} = 3.14\ eV$ and $E_{Diss.}^{Ar,V} = 3.40\ eV$. Exceptions to high dissociation energies are few particular atomic sites just below the edge of the step. If the impurity atoms are trapped from 5:th to 7:th layer vacancies under a step, corresponding dissociation energies are only $E_{Diss.}^{Ar,V} = 0.60 - 0.70\ eV$ and $E_{Diss.}^{Ne,V} = 0.70 - 0.90\ eV$ depending on the release direction. These are clearly lower than any other calculated dissociation energies for these impurities trapped at monovacancies.

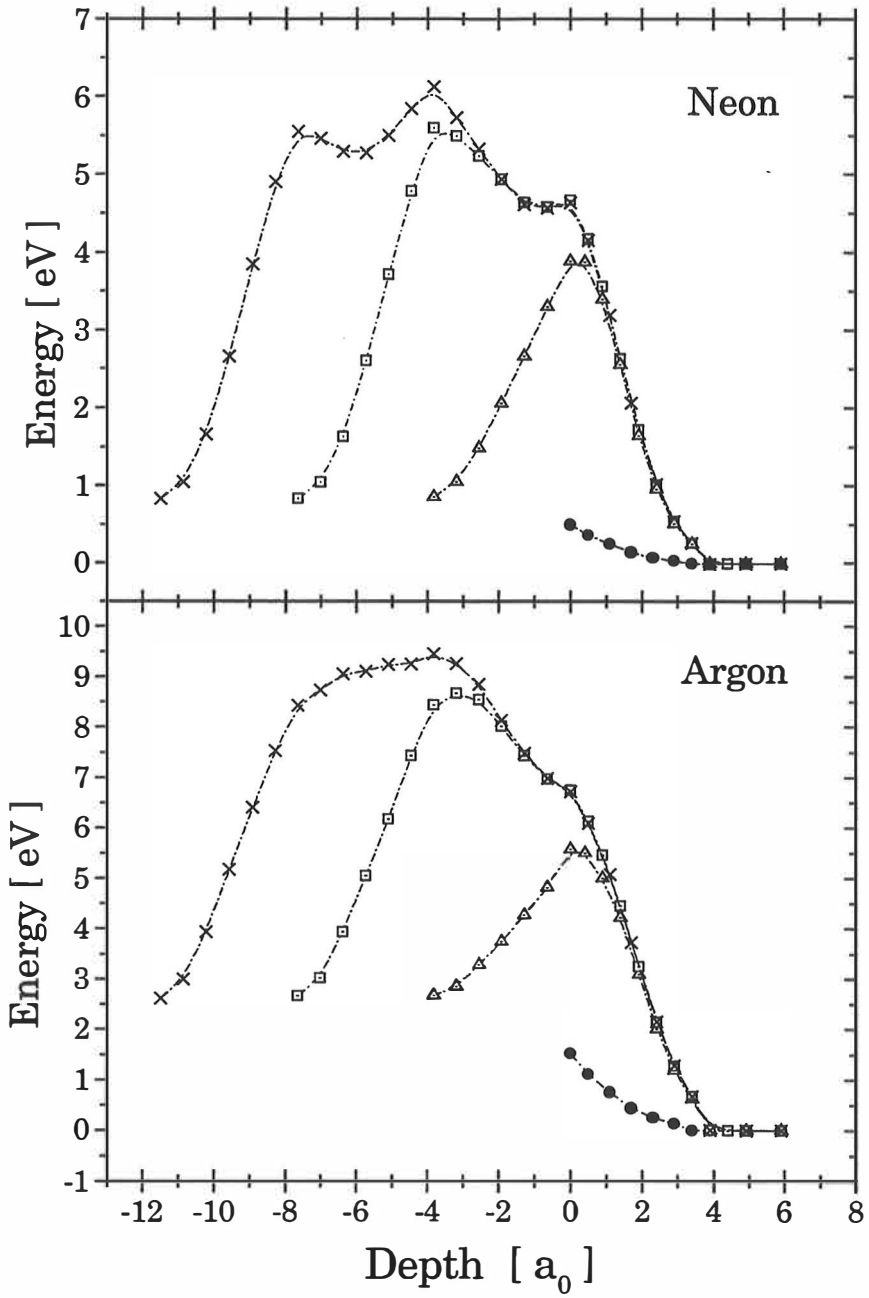

Figure 5.10. *Potential barriers for the dissociation of neon and argon atoms that are trapped at vacancies near (111) surface. Four different curves show dissociation barriers in first, second, third and fourth layer vacancies.*

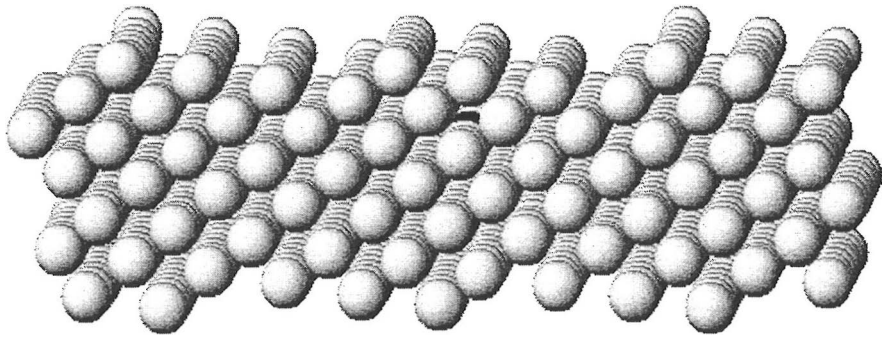

Figure 5.11. *Relaxation around argon in 9:th layer vacancy in (340)-surface is small. This relaxation however prevents the surface inward relaxation of the edge in the step. Argon atom is denoted by black color.*

Dissociation energetics was calculated also for the singly and doubly filled divacancy and for a monovacancy that was filled with a few impurity atoms. These calculations were repeated for the same surfaces studied above and computational details were similar.

When a monovacancy was filled with two noble-gas atoms, one of them quickly jumps to the nearest octahedral site and furthermore to the surface where it escapes to the gas phase. In the bulk calculations it was obtained that a monovacancy can be filled with one argon atom, two neon atoms or with three helium atoms. A monovacancy that is near the surface can not be doubly filled with neon or argon. An evident reason for this is the relaxation around the impurity. It generates an open-volume route to the surface if these impurities were originally located in the first few atomic layers. This means that multiple filling of vacancies is not favored close to the surface layers.

When the metal lattice is irradiated with high energies or with high doses, clusters of vacancies and impurities are formed. Impurities are usually trapped strongly by these clusters. In this work we studied only divacancies that are singly or doubly filled with impurities. The only surface at which these energies were calculated

was (340).

Activation energies depend on the depth at which the divacancy is. The result for the dissociation energy for the argon in divacancy is $E_{Diss}^{ArV_2} = 0.17\ eV$ and for the neon in divacancy $E_{Diss}^{NeV_2} = 0.17\ eV$ in the case where the nearest neighbour vacancies are in 12:th and in 5:th atomic layers below the (340)-surface. In the neon case there seems to be also another minimum in the potential curve, corresponding to an activation energy of $E_{Diss}^{NeV_2} = 0.13\ eV$. If either of the vacancies is in 4:th atomic layer or closer to the surface there is no trapping. This is expected since in these cases there is an open route to the surface. If the divacancy is deeper in, the dissociation energies are somewhat higher. There are however some exceptions. If either of the vacancies is below the edge of a surface step, then dissociation energies are $E_{Diss.}^{ArV_2} = 0.20\ eV$ and $E_{Diss}^{NeV_2} = 0.21eV$, in the case where vacancies are at the 2:nd and 9:th atomic layers. Dissociation barriers are shown in figure 5.12 for both cases.

The other cluster defect studied was a divacancy filled with two impurity atoms. In these calculations impurity was moved from the upper vacancy to the surface through octahedral sites or directly to the surface depending on the lattice site. In that case dissociation energies are much higher, indicating that the divacancies are stabilized by gas impurities. Dissociation energies are again dependent on the depth at which the vacancies are. When two argon or two neon are in a divacancy so that vacancies are at 20:th and in 13:th atomic layers, the dissociation energies are $E_{Diss.}^{Ar_2V_2} = 3.80\ eV$ and $E_{Diss}^{Ne_2V_2} = 3.70\ eV$. Again differences between argon and neon are small. In that depth the metallic environment is essentially the same as in the bulk and the dissociation energies do not change any more if defects are deeper in the lattice. If the vacancies of the divacancy are in the 15:th and in the 8:th atomic layers, the dissociation energy for the upper impurity is $E_{Diss.}^{Ar_2V_2} = 2.80\ eV$ for argon and $E_{Diss}^{Ne_2V_2} = 2.90\ eV$ for neon. Potential barriers corresponding these two cases are shown in figure 5.13. Note that again the dissociation energy for neon is slightly higher than that for argon. If either vacancy is higher than in the eight atomic layer, the impurity is free.

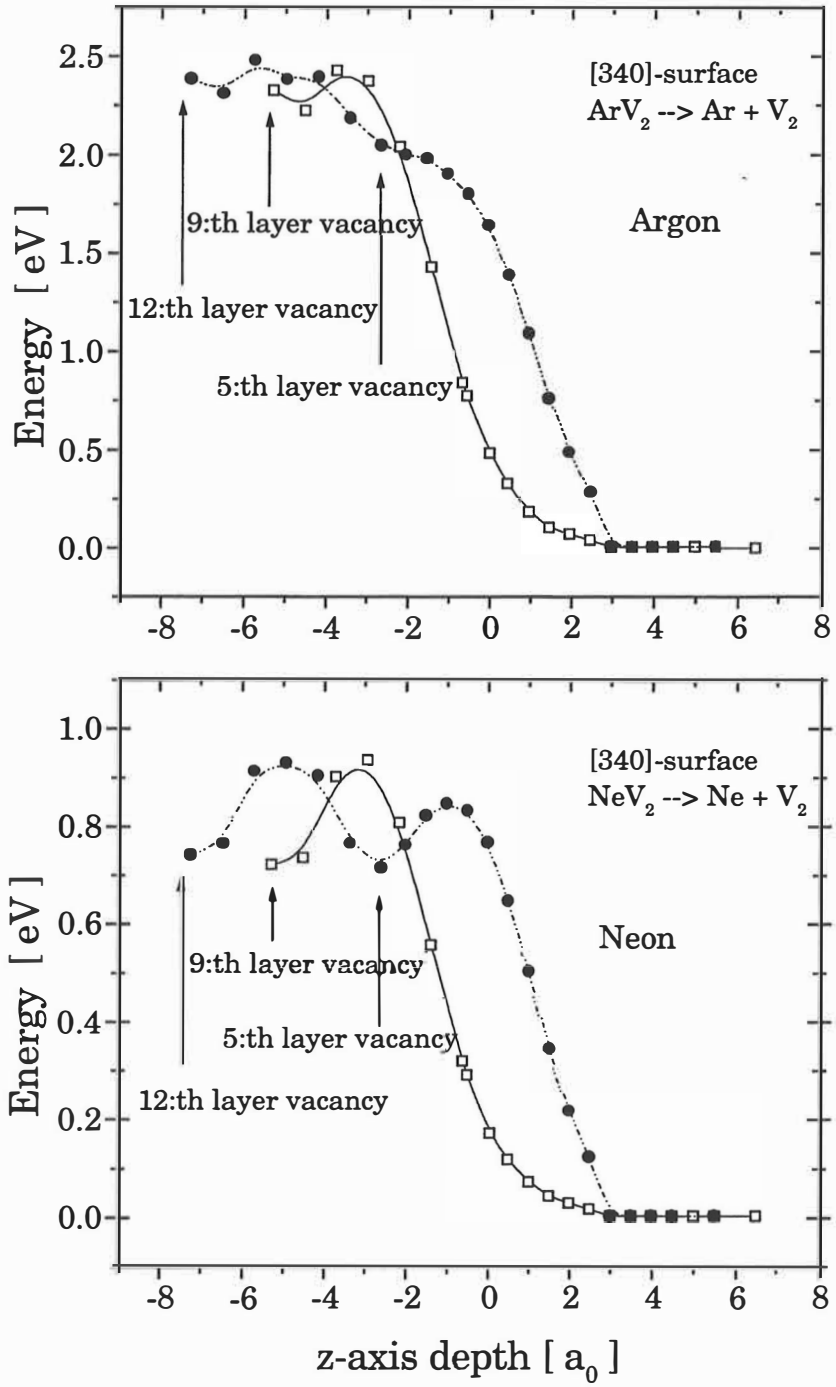

Figure 5.12. *Potential barrier for the dissociation when argon or neon is trapped in 12:th-5:th layer divacancy and in 9:th-2:nd layer divacancy near the tip of the surface step.*

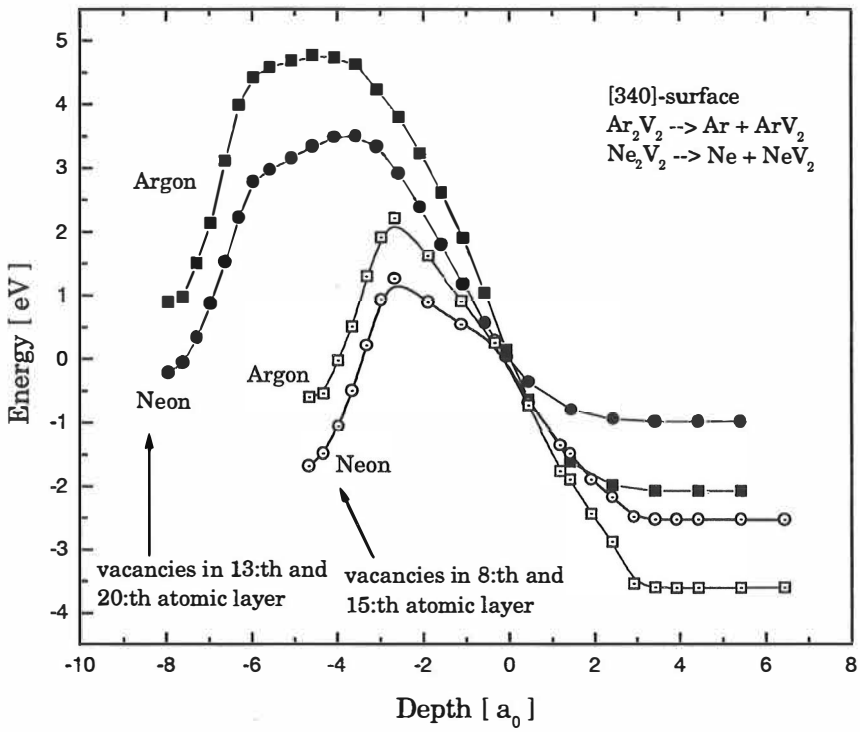

Figure 5.13. *Potential barrier for the dissociation when two argon or two neon is trapped in 20:th-13:th layer divacancy and in 15:th-8:th layer divacancy.*

The last studied phenomena was vacancy migration in copper. This was done simply by moving one copper atom from an ideal lattice site to nearest neighbour vacancy and allowing other neighbouring atoms to relax freely toward equilibrium site. This calculation was done in bulk conditions. The resulting migration energy in copper was $E_V^{mig.} = 1.3\,eV$. This is smaller than most of the calculated dissociation energies, suggesting that neon and argon impurities could be released via moving vacancies. Figure 5.14 shows the potential barrier for the vacancy migration.

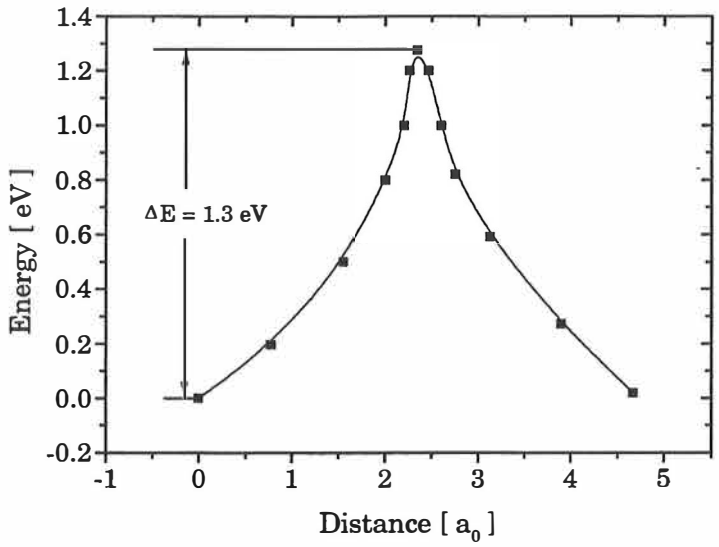

Figure 5.14. *Potential barrier for the vacancy migration in copper according to effective-medium theory. Calculation do not take account temperature related effects. Migration energy is* $E_V^{mig.} = 1.3\ eV$. *Sub-index V refers to vacancy.*

In conclusion, the results show that dissociation energies at different surfaces are strongly dependent on the surface geometry, on the site where atom breaks the surface and on the packing density of the surface. Furthermore, there is so many possible processes and reaction paths which has similar activation energies that it is expected that in the desorption spectra the corresponding peaks are overlapping. High dissociation energies for the impurity trapped at a monovacancy suggest that there are alternative release methods. One possibility is that heavier impurities are released via moving vacancies.

6. Identification of the peaks in the desorption spectra

6.1 Helium peaks

Helium desorption from copper can be understood relatively well. Measurements show dependencies that are clear indicators of different processes. Most of the helium peaks can be explained purely by means of experimental results. Theoretical results for the binding and dissociation energies agree well with such predictions.

Totally five different peaks were found in helium desorption spectra. The most significant peak in every spectrum is the peak labeled with H (see figure 6.1). This peak is due to single helium atoms that are released from monovacancies. This can be concluded from the dose and energy dependencies related to this peak (see chapter 3). There is also a sharp threshold energy, which is characteristic for impurity release from monovacancies. A vacancy-interstitial pair should also be the most common defect caused by irradiation with a helium beam. Application of the peak analysing methods gives an activation energy $E_D = 2.1\ eV$ and the peak shape follows exactly to first order kinetics. Model calculations that have been done with the effective-medium theory, give a dissociation energy $E_{HeV}^{Diss.} = 2.17\ eV$ for helium trapped in a monovacancy. This agrees well with the measured value. When all the information is combined together, there is hardly doubt that this peak is due to the helium atoms that have been released from monovacancies and migrate to the surface where they are detected.

Migration energy of helium in copper estimated from the measurements is $E^{mig.} = 0.36\ eV$. The theory gives a result of $E^{mig.} = 0.50\ eV$ for both of the octahedral-octahedral and tetrahedral-octahedral migration jumps. If the diffusion peak position is approximated with the kinetic equation the effect of diffusion should be seen in the beginning of the spectra at the temperature range of $150 - 300\ K$. There

are usually two peaks in the beginning of the spectra. The first peak is expected to be caused by the release of helium atoms that are trapped to interstitial positions near the surface. In this case the migration energies are smaller than in the bulk as can be seen from theoretical results for neon and argon. In addition, the low-temperature peak contains helium atoms that are released from the sample support pins and from the oven. This can be concluded from the measurement where the oven was bombarded with the helium beam and the release was measured with the mass spectrometer. This was the only observed peak in that case.

Since helium is a small impurity, it is likely that with larger irradiation doses and energies there are also monovacancies that are multiple filled. According to calculations it is possible to occupy a vacancy with three helium atoms. These defects can cause several peaks, since dissociation of these defects occurs in several separate steps. Energies are lower than the monovacancy-helium dissociation energy. For that reason there should be at least two peaks in the spectra which are due to the multiple filling of monovacancies. These peaks correspond to two different dissociation schemes: $He_3V \rightarrow He_2V + He$ and $He_2V \rightarrow HeV + He$. The two peaks might also be so close that they could be seen as one broad peak. This can be expected according to theoretical model calculations, which give dissociation energies of $E^{Diss.}_{He_2V} = 1.75\ eV$ and $E^{Diss.}_{He_3V} = 1.45\ eV$ for these processes. The theory suggests that those peaks should be seen at the low temperature side of the monovacancy peak. In fact, there are two peaks, labeled with G and X which are near the H peak. The peak temperatures are around 540 K and 600 K. Peak G is strongly dependent on the irradiation dose. In addition, when the dose increases, the peak width increases and finally there are clearly two overlapping peaks in the spectrum. These two peaks are interpreted as doubly and triply occupied monovacancies. The calculated dissociation energies are in good agreement with this interpretation.

The peak labeled with X is seen only at high irradiation energies at the shoulder of the H peak. This peak is however almost independent of the irradiation dose and it is seen already at low dose. These dependencies led to the conclusion that the X peak is due to the singly occupied divacancy. One problem, however, is the desorption temperature. It is relatively high for such a defect. In principle, a

divacancy which is occupied with only one helium atom should be mobile already at lower temperatures, since the calculated migration energy for a monovacancy in copper is 1.3 eV. This means that this defect type should move with a vacancy migration process where the impurity jumps to one vacancy while the other vacancy jumps to the nearest neighbour position and so on. An alternative reaction path could be a direct escape of the helium atom from the divacancy. However, the activation energy of this process should be higher than the activation energy for vacancy migration. There are some estimates for dissociation energies in such case [38]. According to these the energy is not significantly different from the activation energy for helium release from a monovacancy. When all the information is combined together, it is most likely that the X peak represents helium release from a divacancy, which occurs via dissociation mechanism.

When the irradiation energies and the doses are of the order of 10 keV and 10^{14} $ions/cm^2$, a broad peak appears at high temperatures. The need of high energy and dose indicate that this peak is due to vacancy clusters containing three or more vacancies.

There is one peak in the helium spectra which has not yet been explained. This peak is seen around the temperature of 380 K. This peak does not depend on the dose and on the irradiation energy at all. The peak temperature is so low that it fits to the case where impurities are trapped in mono- and in divacancies near the surface. In both cases the calculated energies are quite low, assuming that impurities are released via vacancy migration mechanism.

6.2 Neon and argon peaks

In general, peaks in the argon and in neon spectra can not be identified with help of the experimental results alone. The main reason is that the peaks are wider and the dose and energy dependencies are weak. However, combining results of theoretical modelling and results of desorption measurements, at least some of the peaks can be explained.

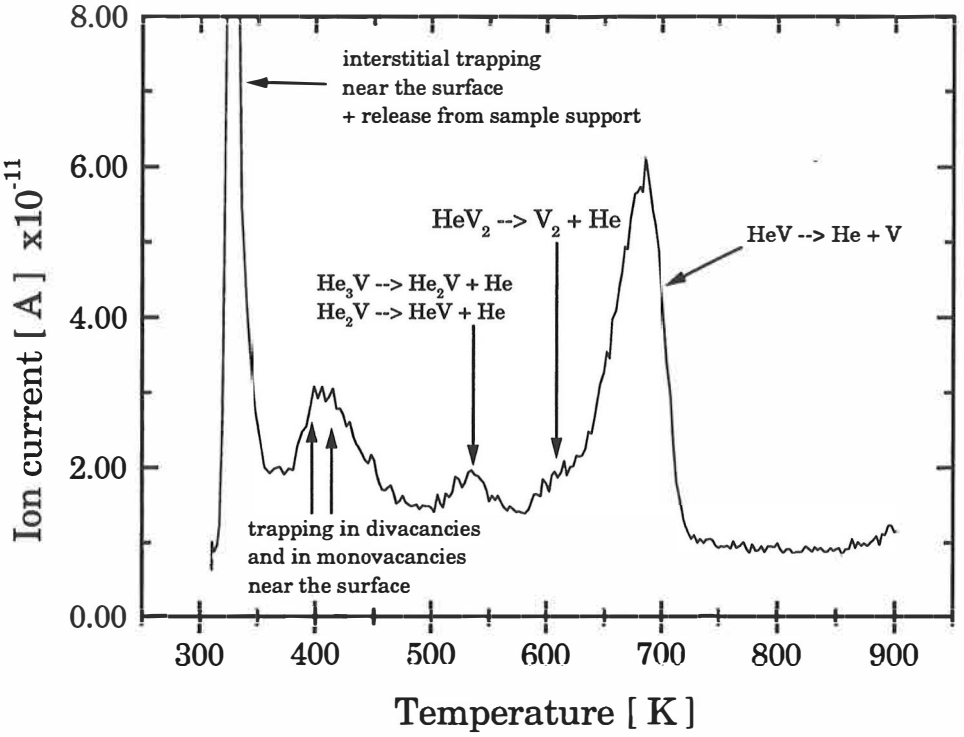

Figure 6.1. *Identification of the peaks in helium desorption spectra from copper. Predictions are made by combining experimental and theoretical results.*

Both argon and neon spectra have four or five different peaks at the temperature range from 200 K to 800 K. The first peak is seen around 200 K and is clearly the same peak that is present in helium spectra. The peak temperature varies slightly depending on the irradiation conditions. This peak is due to the interstitial impurity release and due to the release of neon and argon from the sample support pins and oven.

The next two argon peaks are observed at the temperature of 250 K and 350 K. These peaks are visible only when the irradiation energy is below 1 keV. These peaks can not be explained by means of desorption measurements since energy and dose dependencies are not clear at all. When the energy is increased, these

peaks are overlapping more and more and finally there is only one broad peak at the temperature of 280 K. This peak is a combination of at least two different phenomena occuring near the surface. The only low activation energies that were found in modelling were the dissociation of near surface divacancies filled with one impurity atom. There are several activation energies corresponding different dissociation sites near the surface. A natural conclusion is that both of these peaks represent dissociation of near surface divacancies occupied with one argon atom. The same peak combination is seen also in the neon spectra. The temperature range and the overall behavior is the same in both cases.

More interesting phenomena are seen in neon and argon spectra at intermediate temperatures. In both spectra there is a clear double peak. In the argon spectra the peak temperatures are 485 K and 570 K while in the neon spectra they are 550 K and 660 K. These peaks have been explained earlier by the impurity release from singly occupied divacancies and by the release of impurities from singly occupied monovacancies. Another suggestion has been that the peaks represent release of impurities from monovacancies at different depths [6,24,39]. In the latter case it was assumed that the lower temperature peak is due to the surface traps and the higher temperature peak due to the traps located deeper in the crystal. Arguments for those interpretations are energy and dose dependencies that are clearly seen in measurements. However, there are problems concerning peak temperatures as well as shapes and intensities. The peaks are at lower temperature than that of the helium H-peak, which is seen at the temperature of 700 K. This would mean that the activation energies are lower for the heavier atoms. This is not in agreement with the theory which gives much larger dissociation energies for neon and argon than for helium. Another discrepancy is the peak height. Since the penetration range of large ions is small, peaks which represent processes that are occuring deeper in the crystal should be lower than peaks related to near-surface processes. However, peaks are symmetric. This suggest that the corresponding reaction does not obey first-order kinetics, but more likely the kinetic order of the reaction is two. This fits to the case where impurity atoms are released from defects via mobile vacancies, since the release rate is dependent on the concentrations of

vacancies and on the concentrations of impurities. Also, the energy dependence of the high temperature peak gives a hint that this peak is related to the di- or trivacancies, since the peak intensity is increasing with increasing irradiation energy. The low temperature peak does not have such a dependence on the energy. This would imply that the origin of the peak is related to the impurity release from a singly filled monovacancy. If this is the case the release mechanism must be vacancy-assisted, to explain the low activation energies. Another explanation to the low temperature peak are defects located near the surface. According to our calculations the activation energy for direct impurity dissociation from singly filled monovacancy near the surface is only $0.6 - 0.7\ eV$ for argon and $0.7 - 0.9\ eV$ for neon. Indeed, desorption spectra show argon peaks at lower temperature than neon peaks.

Combining experimental and theoretical results, the best interpretation of the double peaks in the argon and in neon spectra is direct noble-gas impurity release from singly filled monovacancies that are located near the surface (lower temperature peak) and noble-gas impurity release from divacancies located deeper in the crystal (higher temperature peak). The latter process is then vacancy-assisted, which means that mobile divacancies are carrying the noble gas atoms to the surface.

When the irradiation energies and doses are high enough, the characteristic double peak is replaced by a broader distribution. This distribution is clearly caused by multiply filled defects with several impurities trapped in a vacancy cluster. The arguments for this explanation are the strong energy and dose dependences and the fact that this distribution is seen only with high energies and doses.

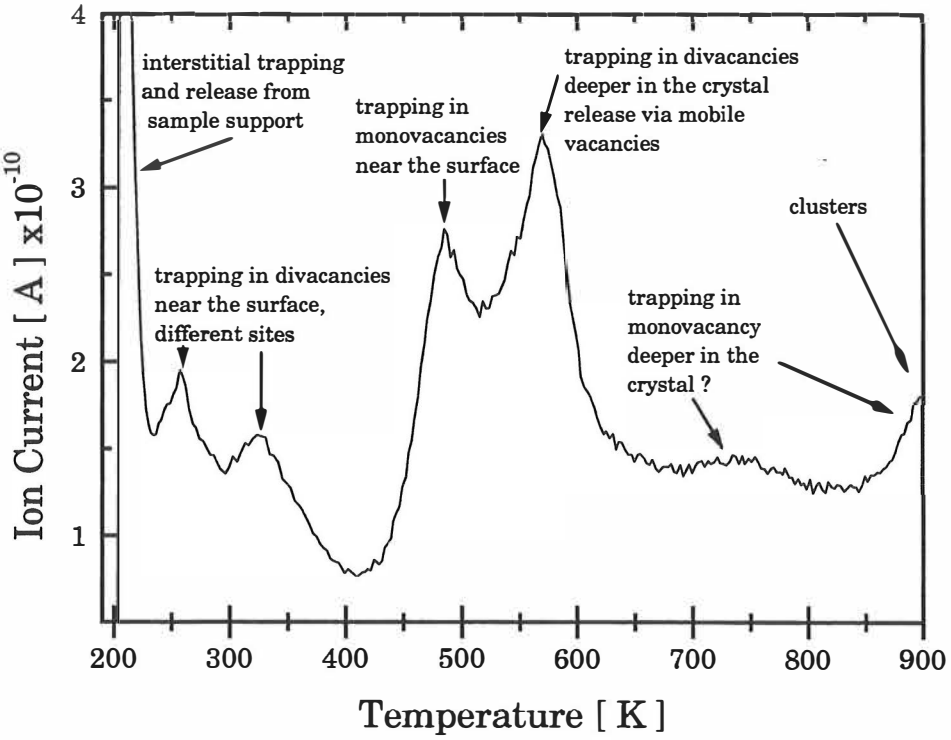

Figure 6.2. *Identification of the peaks in argon desorption spectra from copper. Predictions are made by combining experimental and theoretical results. In neon spectra the peaks that are seen are just the same than peaks in argon spectra.*

7. Summary

This thesis is a review of the work where properties of noble gas implants in copper have been studied experimentally and theoretically. The experimental work utilizes the sophisticated thermal desorption method. This part of the work includes measurements as well as the analysis of the measured peaks. During the work almost 500 helium, neon and argon bombardments in copper were done and the desorption spectra were measured. Most of the peaks observed in these spectra were analyzed with various methods. Some new methods for desorption peak analysing were developed.

Theoretical modelling work was done using the effective medium theory. This includes parameter determination for total energy calculations. These parameters were calculated from the results of *ab initio*-electronic structure calculations. The parameters were then used in a total energy program to study migration and trapping of the noble gases in copper, both in the bulk and close to a surface. The results were used in the interpretation of the experimental desorption spectra.

Quite complete picture about the helium behavior in copper was obtained. It was clearly demonstrated that helium traps at vacancies and is released when temperature is raised enough. It was found that this kind of helium release follows first-order kinetics. All the peaks obtained in helium desorption spectra were identified and explained in detail. Some of the measurements were done also with the ^3He isotope. The results suggest that the isotope effect shifts the peak temperatures slightly. All the helium peaks were analyzed with different analysing methods. When this was done it was noted that all the peaks should be analyzed with at least two or three independent methods so that the analysis does not fail and that the accuracy of the resulted activation energies can be estimated. New reliable and practical methods were developed to first order peak analysis.

Experiments done with neon and argon show a few interesting results, such as double peaks in intermediate temperatures. It was noted, however, that the inter-

pretation of those peaks is not straightforward due to the peak shapes, relatively low temperatures and due to the different energy-dose dependencies. Surprisingly, neon peaks were at higher temperatures than the corresponding argon peaks.

The total energy calculations that were carried out for helium trapped at vacancies agree well with the measurements. According to the calculations migration of helium goes through interstitial sites and it does not matter whether the migration route is the octahedral-octahedral or the octahedral-tetrahedral path. Calculations also gave the result that a copper vacancy can be filled with up to three helium atom. The migration energy and in some cases also the dissociation energy for neon was higher than that for argon, in qualitative agreement with the experimental results. The calculated minimum energy sites for interstitial argon and neon were different: for argon it is an off-centered octahedral site while neon sits in the center of the octahedral site.

In the case of neon and argon, the total energy calculations were extended to surfaces. The results suggest that the preferred release method for the neon and argon trapped in a vacancy near the surface is the release via mobile vacancies. It was noted that dissociation energies for near surface defects are strongly dependent on the surface orientation and on the geometry and purity of the surface. Moreover, in stepped surfaces the dissociation energies are dependent on the site where impurity breaks the surface.

References

[1] H. Ullmaier, Nucl. Fusion **24**, 1039 (1984)

[2] V.N Chernikov, J. Nucl. Materials, **195** (1992) pp.29-36

[3] E.V. Kornelsen, Can. J. Phys. **48**, 2812 (1970)

[4] E. V. Kornelsen, Radiat. Eff. **13**, 227 (1972)

[5] S. K. Erents and G. Charter, J. Appl. Phys. **1**, 1323 (1968)

[6] E. Kautto, Research report No. 4/1995,Department of Physics, University of Jyväskylä, 1995 (Ph. D. thesis)

[7] A. A. van Gorkum and E. V. Kornelsen, Vacuum bf 31, 89 (1981)

[8] A. van Veen, Materials Science forum **15 - 18**,3 (1987)

[9] E. Kautto, J. Kuhalainen and M. Manninen, Phys. Scr., Vol. 55,**5**, pp. 628-633 (1997)

[10] J. Kuhalainen, M. Manninen and E. Kautto, J. Phys.:Condens. Matt. **8**, 10317-10326 (1996)

[11] O. B. Christensen, P. Stolze, K. W. Jacobsen and J. K. Nørskov, Phys. rev. B **41**, 12413 (1990)

[12] M. J. Puska in *Many atom interactions in solids* (Springer Proceedings in Physics 48),1990, ed. R. M. Nieminen, M. J. Puska and M. Manninen, pp. 134-143

[13] K. W. Jacobsen, J. K. Nørskov and M. J. Puska, Phys. Rev. B **35**, 7423 (1987)

[14] O. B. Christensen, K. W. Jacobsen, J. K. Nørskov and M. Manninen, Phys rev. Lett. **66**, 2219 (1991)

[15] J. L. Falconer and R. J. Madix, Surf. Sci. **48** 393 (1975)

[16] P. A. Redhead, Vacuum **12**, 203 (1962)

[17] G. Carter, Vacuum **12**, 245 (1962)

[18] J. Kuhalainen, Laboratory report 2/1994, Department of Physics, University of Jyväskylä, 1994, in Finnish (Ph. Lic. thesis)

[19] J. E. Hoogenboom, W. de Vries, J. B. Dielhof and A. J. J. Bos, J. Appl. Phys **64**,6 (1988)

[20] E. Kautto, O-P. Kähkönen, J. Kuhalainen and M. Manninen, Nucl. Instr. Meth. B, **103**, 376-382 (1995)

[21] E. V. Kornelsen and A. A. van Gorkum, Vacuum **31**, 99 (1981)

[22] E. V. Kornelsen and D. L. Blair, J. Vac. Sci. Technol., **14**, 1299 (1977)

[23] A. van Veen, A Warnaar and L. M. Caspers, Vacuum **30**, 109 (1980)

[24] E. Kautto, J. Kuhalainen and M. Manninen, J. Phys.:Condens. Matt.,**21**, pp. 4365-4376 (1997).

[25] P. Ehrhart, K. H. Robrock and H. R. Schober, in *Physics of Radiation Effects in Crystals*, Volume 13 of *Modern Problems in Condensed Matter Sciences*, edited by R. A. Johnson and A. N. Orlow (North-Holland, Amsterdam, 1986) p. 3

[26] J. F. Ziegler, J. P. Biersack and U. Littmark 1985, *The Stopping and Range of Ions in Solids*, Pergamon Press, New York and *The Transport of Ions in Matter* (TRIM-96), Instructions

[27] W. Th. M. Buters, A. van Veen and A. van den Beukel, Phys.Stat. Sol. (a) **100**, 87 (1987)

[28] D. J. Edwards, Jr., J. Appl. Phys. **46**, 1444 (1975)

[29] U. Yxklinten, J. Hartford and T. Holmquist, Phys. Scr.,Vol. 55, 499-506 (1997) Calculated parameters and data is available in http://fy.chalmers.se/ hart/

[30] *Interatomic Potentials and Simulation of Lattice Defects*, eds. p.C. Gehlen, J. R. Beeler and R. I. Jaffee, Plenum Press, New York (1972)

[31] J. R. Beeler Jr.,*Radiation effects computer experiments*, (series Defects in

Crystalline Solids, eds. S. Amelinckx, R. Gevers and J. Nihoul), North-Holland Publishing Company (1983)

[32] L. Hedin and B. Lundquist, J. Phys. **C4**, 2064 (1971)

[33] O. Gunnarsson and B. Lundquist, Phys. Rev. B **13**, 4274 (1976)

[34] D.M. Ceperley and B.J. Alder, Phys. Rev. Lett. 45, 566 (1980).

[35] J.P. Perdew and A. Zunger, Phys. Rev. B **23**, 5048 (1981)

[36] J. P. Perdew and Y. Wang, Phys. Rev. B **33**, 8800 (1986)

[37] J. P. Perdew and Y. Wang, Phys. Rev. B **45**, 13244 (1992).

[38] W. D. Wilson, M. I. Baskes and C. L. Bisson, Phys. Rev. B **13**, 2470 (1976)

[39] D. J. Edwards, Jr., J. Appl. Phys. **46**, 1437 (1975)

[40] R. Chen, J. Appl. Phys. **40**, 570 (1969)